NUREG/CR-2774 Vol. II
ANL-82-24 Vol. II

NUREG/CR-2774 Vol. II
ANL-82-24 Vol. II

PHYSICS OF REACTOR SAFETY

Quarterly Report
April—June 1982

ARGONNE NATIONAL LABORATORY, ARGONNE, ILLINOIS

Prepared for the Office of Nuclear Regulatory Research
U. S. NUCLEAR REGULATORY COMMISSION
under Interagency Agreement DOE 40-550-75

The facilities of Argonne National Laboratory are owned by the United States Government. Under the terms of a contract (W-31-109-Eng-38) among the U. S. Department of Energy, Argonne Universities Association and The University of Chicago, the University employs the staff and operates the Laboratory in accordance with policies and programs formulated, approved and reviewed by the Association.

MEMBERS OF ARGONNE UNIVERSITIES ASSOCIATION

The University of Arizona
Carnegie-Mellon University
Case Western Reserve University
The University of Chicago
University of Cincinnati
Illinois Institute of Technology
University of Illinois
Indiana University
The University of Iowa
Iowa State University
The University of Kansas
Kansas State University
Loyola University of Chicago
Marquette University
The University of Michigan
Michigan State University
University of Minnesota
University of Missouri
Northwestern University
University of Notre Dame
The Ohio State University
Ohio University
The Pennsylvania State University
Purdue University
Saint Louis University
Southern Illinois University
The University of Texas at Austin
Washington University
Wayne State University
The University of Wisconsin-Madison

Available from

GPO Sales Program
Division of Technical Information and Document Control
U. S. Nuclear Regulatory Commission
Washington, D.C. 20555

and

National Technical Information Service
Springfield, Virginia 22161

NUREG/CR-2774 Vol. II
ANL-82-24 Vol. II

(Distribution
Code: R7)

ARGONNE NATIONAL LABORATORY
9700 South Cass Avenue
Argonne, Illinois 60439

PHYSICS OF REACTOR SAFETY

Quarterly Report
April—June 1982

Applied Physics Division
Components Technology Division

July 1982

Previous reports in this series

ANL-81-29 (II)	April—June 1981
ANL-81-29 (III)	July—September 1981
ANL-82-19 (IV)	October—December 1981
ANL-82-24 (I)	January—March 1982

Prepared for the Division of Reactor Safety Research
Office of Nuclear Regulatory Research
U. S. Nuclear Regulatory Commission
Washington, D. C. 20555
Under Interagency Agreement DOE 40-550-75

NRC FIN Nos. A2015 and A2045

PHYSICS OF REACTOR SAFETY

Quarterly Report
April-June 1982

ABSTRACT

This Quarterly progress report summarizes work done during the months of April-June 1982 in Argonne National Laboratory's Applied Physics and Components Technology Divisions for the Division of Reactor Safety Research of the U.S. Nuclear Regulatory Commission. The work in the Applied Physics Division includes reports on reactor safety modeling and assessment by members of the Reactor Safety Appraisals Section. Work on reactor core thermal-hydraulics is performed in ANL's Components Technology Division, emphasizing 3-dimensional code development for LMFBR accidents under natural convection conditions. An executive summary is provided including a statement of the findings and recommendations of the report.

FIN No.	Title
A2015	Reactor Safety Modeling and Assessment
A2045	3-D Time-dependent Code Development

TABLE OF CONTENTS

LIST OF FIGURES

LIST OF FIGURES (cont.)

LIST OF TABLES

EXECUTIVE SUMMARY

A comparison was made of reactivity feedbacks calculated by EPIC and by PLUTO2 for a 10 ¢/s TOP in the EOC-3 core of the CRBR. It was found that if, in the heat transfer coefficient between molten fuel and sodium, based in both codes on the Cho-Wright model, there was a factor proportional to the first power of the liquid sodium volume fraction, EPIC gave much more negative fuel feedback than PLUTO2 did. If the volume fraction in this factor was squared, however, the EPIC and PLUTO2 results were in fairly good agreement. Apparently use of the squared volume fraction compensated in the case of EPIC for the lack of an annular flow regime, provided by PLUTO2 for lower sodium volume fractions.

Results for fuel motion reactivity were found to be quite sensitive to the pin pressure at failure. For a failure pressure in the range 100-200 atm, this reactivity turns from positive to negative because of fuel sweepout in 30 to 40 msec. In order for the effect to turn negative in about 15 msec a failure pressure of 600 atm was found necessary, according to EPIC with use of the sodium volume fraction squared factor. Considerations of clad strength and possible failure mechanisms make a failure pressure in the range 100-200 atm seem more likely, however.

In the previous quarterly report it was found that for the CRBR EOC-3 core autocatalytic conditions were being attained in a TOP accident with an assumed core midplane failure and a relatively weak fuel sweepout for a ramp rate as low as 10 ¢/s. It has since become evident that because of deficiencies in the SAS3D calculation of the time variation of fuel melt fraction, used as a pin failure criterion, the coherence of failure was being considerably overestimated. These deficiencies were removed by use of a pin enthalpy failure criterion. With this criterion it is found that with weak fuel sweepout developing over to 20-40 msec autocatalytic conditions are not being attained until the ramp rate is in the vicinity of 20 ¢/s.

The BIFLO code for multidimensional analysis of sodium boiling has been modified to adjust array dimensions to the minimum size needed and to add an inlet velocity boundary condition. Loss-of-flow calculations performed for various bundle sizes are indicating that the dividing line between one- and two-dimensional behavior is a complex function involving more characteristics than just the physical bundle size. Initial calculations of events following the sudden total blockage of the inlet flow area of a fuel assembly are indicating that the upper half of the core becomes highly voided of sodium very rapidly following initiation of boiling at the core centerplane.

In the case of COMMIX-1A development work, most efforts were devoted to documentation. Most of the sections of COMMIX-1A report are completely written and are now being typed.

In the area of validation of COMMIX for preparation of CRBR licensing, the FFTF simulation and EBR-II simulation are completed. The reports on these simulations are prepared. They are:

(i) "COMMIX-1A Three-Dimensional In-Vessel Simulation of the FFTF Thermal Hydraulics," by S. P. Vanka, H. M. Domanus, and W. T. Sha, ANL-CT-82-1 (January 1982).

(ii) "COMMIX-1A Three-Dimensional In-Vessel Simulation of the FFTF Transient Thermal Hydraulics," by S. P. Vanka, H. M. Domanus and W. T. Sha, ANL-CT-82-14 (July 1982).

(iii) "EBR-II In-Vessel Natural-Circulation Analysis," by W. L. Baumann, H. M. Domanus, D. Mohr, W. T. Sha, R. C. Schmitt, and J. E. Sullivan, ANL-CT-82-19.

The resimulation of German Seven-pin transient confirmed that modifications and improvement implemented in COMMIX-2 has not introduced any errors.

To test the new-pressure scheme implemented in BODYFIT code, the problem "Flow in a 90°-Bend Elbow" was resimulated. The results show a significant improvement in the convergence rate.

I. REACTOR SAFETY MODELING AND ASSESSMENT

(A2015)

A. LMFBR Accident Studies

1. Comparison of Reactivity Feedback Calculated by EPIC and PLUTO2 for TOP Accidents in the CRBR (H. H. Hummel and P. A. Pizzica

A comparison of fuel and sodium fuel motion feedbacks has been made between the EPIC code[1], incorporated in SAS3D/EPIC, and PLUTO2[2], incorporated in SAS4A, for slow TOP-type failure in channel 10 of the EOC-3 core[3] of the CRBR. In the comparisons the power in general rose to a few times normal, based on a 10 ¢/s reactivity ramp rate. The power histories varied somewhat from one calculation to another, but this should not affect the validity of the comparisons significantly because the calculated feedbacks were not very sensitive to the pin pressure at the time of failure, one of the important parameters in the study.

TABLE I. Data for CRBR EOC-3 TOP Calculations

Ramp Rate 10 ¢/sec, 20 ¢/sec
1 Node Rip (~7 cm)
No Failure Extension
Fuel Particle Radius 170 μm
FCI Heat Transfer proportional to (NaVF) or $(NaVF)^2$
20% Gas Retention in Equiaxed Fuel
Pin Pressures at Clad Failure - 100, 200, 600 atm
Clad failure at Core Midplane Using Enthalpy Criterion Corresponding to 0.50 Fuel Melt Fraction

Parameters chosen for the calculation are given in Table I. In the item pertaining to FCI heat transfer, the factor NaVF is the liquid sodium volume fraction in the coolant channel, and either this quantity or its square multiplies the fuel-sodium heat transfer coefficient which in both EPIC and PLUTO2 is based on the Cho-Wright parametric model.

General trends found in the studies are as follows:

a. A rapid development of fuel sweepout (in 15 ms or less) with resulting cancellation of positive fuel motion effects occurs only at high pin failure pressure (> 100-200 atm) or with what is probably an unrealistically strong FCI. A high pin pressure at failure appears to have been assumed for the PLUTO2 calculations in GEFR-00523[4].

b. Cancellation of positive fuel reactivity effects occurs later with a weaker FCI, but the effect of FCI parameter variation is relatively more important at lower failure pressures.

c. FCI effects in EPIC are considerably weaker when the fuel-coolant heat transfer coefficient is assumed proportional to the square of the sodium liquid volume fraction rather than to the first power. Both the sweepout reactivity effect and the positive fuel motion reactivity effect, dependent on the amount of fuel ejected, are affected. Development of annular flow for low sodium volume fractions makes the effect of the variation less important for PLUTO2 than for EPIC.

d. EPIC predicts more negative fuel motion reactivity than PLUTO2 does, but the discrepancy is less when the squared liquid volume fraction factor is used.

In Figs. 1 and 2, total fuel motion reactivities calculated by EPIC and PLUTO2 are compared for the linear and squared sodium volume fraction

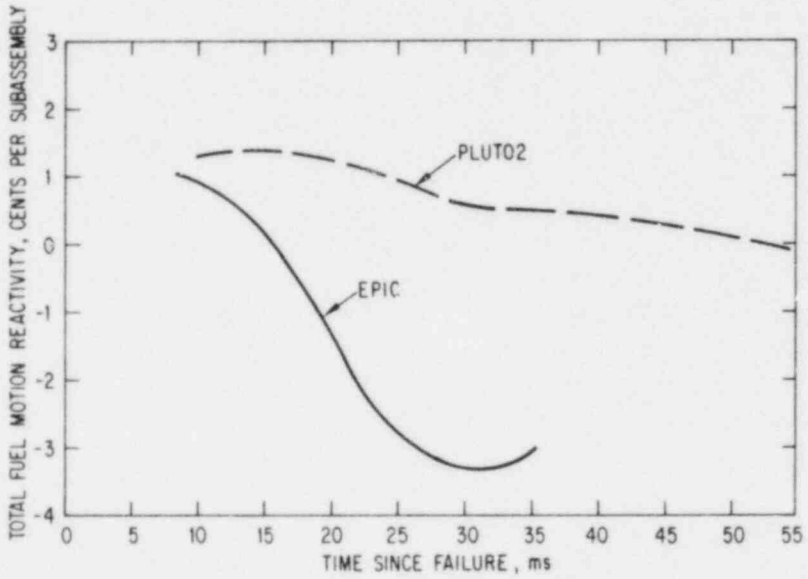

Fig. 1. EOC-3 Channel 10 Total Fuel Motion Reactivity for Fuel-Coolant Heat Transfer Proportional to (NaVF). Failure Pressure 200 atm.

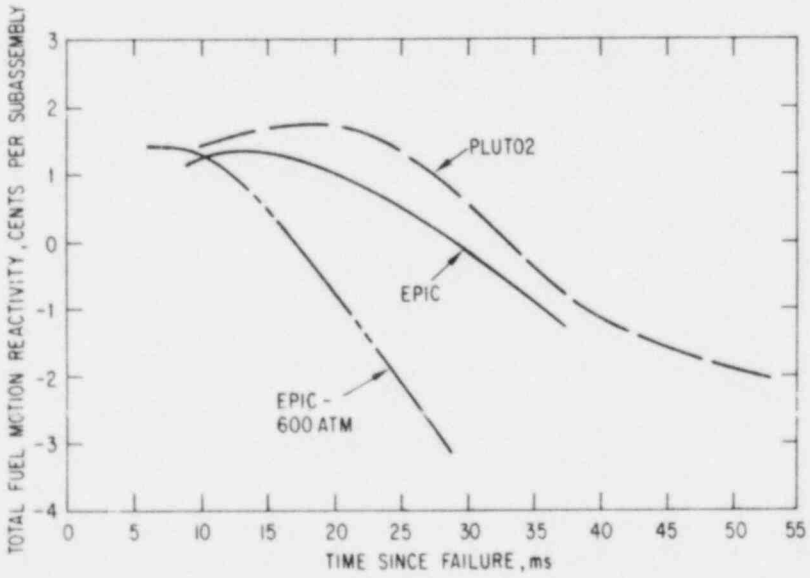

Fig. 2. EOC-3 Channel 10 Total Fuel Motion Reactivity for Fuel-Coolant Heat Transfer Proportional to $(NaVF)^2$. Failure Pressure 200 atm except as noted.

factors. In Figs. 3 and 4 a similar comparison is made for the fuel sweepout reactivity, defined as the reactivity effect caused by fuel motion in the coolant channel. It is seen in these figures that for the assumption of heat transfer proportional to $(NaVF)^2$ there is reasonably good agreement between EPIC and PLUTO2; use of this assumption apparently compensates rather well for the lack of an annular flow model in EPIC, at least in this particular case.

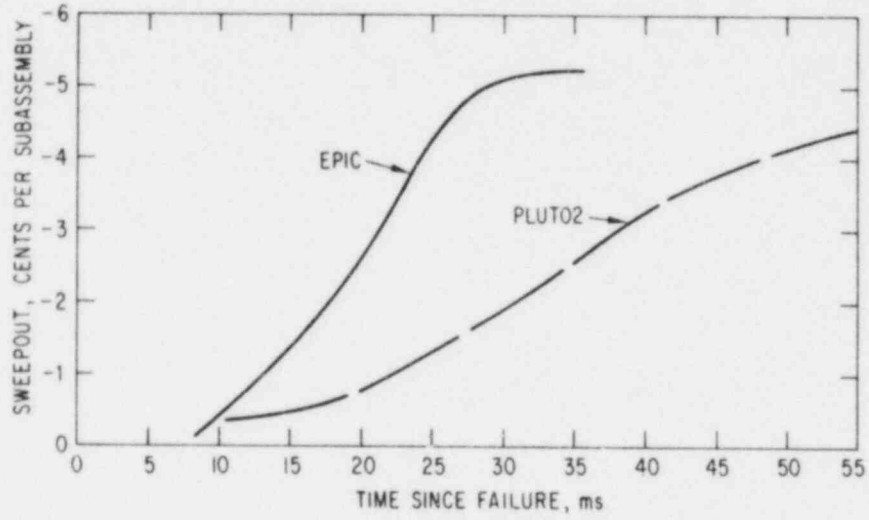

Fig. 3. EOC-3 Channel 10 Sweepout Reactivity for Fuel-Coolant Heat Transfer Proportional to (NaVF). Failure Pressure 200 atm.

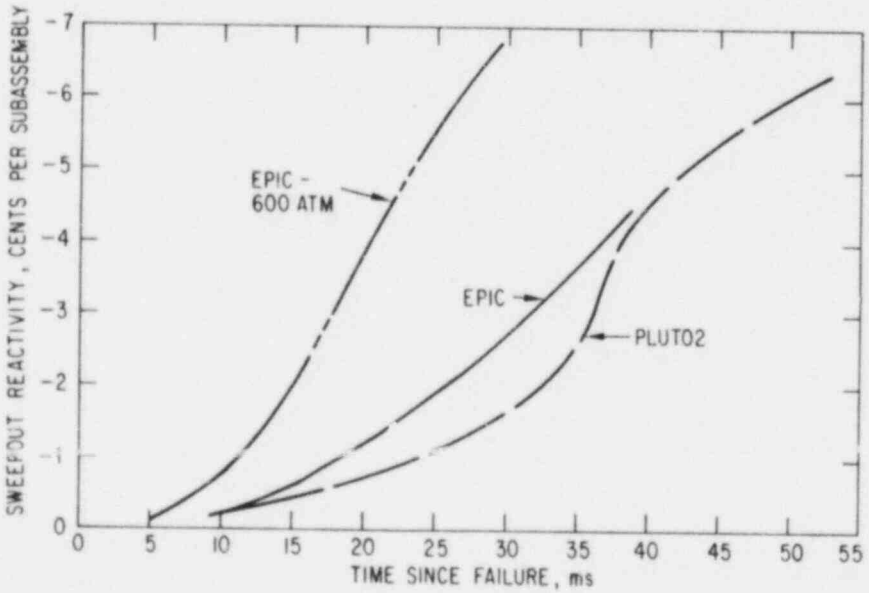

Fig. 4. EOC-3 Channel 10 Sweepout Reactivity for Fuel-Coolant Heat Transfer Proportional to $(NaVF)^2$. Failure Pressure 200 atm except as noted.

For heat transfer proportional to (NaVF), the disagreement for total fuel motion reactivity between EPIC and PLUTO2 is even larger than that corresponding to the difference in sweepout reactivity because the higher FCI pressure in the EPIC case reduces molten fuel ejection into the coolant channel, thereby reducing the positive reactivity effect from inpin fuel motion to the failure point. The sweepout reactivity is still larger for EPIC even with the reduced fuel ejection because of the higher fuel velocity in the coolant channel corresponding to the higher pressure.

In Table II the fuel motion and also sodium motion reactivity effects are compared for the available cases at 15 and 30 msec following pin failure. The longer time scale of events for 100 atm failure pressure compared to the times for higher pressure cases is evident in this table.

TABLE II. Comparison of EPIC and PLUTO2 Reactivities, CRBR EOC-3 Core, 10 ¢/sec TOP, Channel 10, Particle Radius 170 μm

Code	Failure Pressure (atm)	X in $h_{fc} \sim (NaVF)^X$	Sodium Motion Reactivity (Cents/Subassembly)		Fuel Motion Reactivity (Cents/Subassembly)			
					Sweepout		Total	
			15 ms	30 ms	15 ms	30 ms	15 ms	30 ms
EPIC	100	1	0.8	1.0	-0.4	-3.4	0.4	-2.8
		2	0.8	0.8	-0.2	-1.0	1.2	0.8
PLUTO2	100	2	0.6	0.8	-0.4	-1.4	1.1	0.6
EPIC	200	1	0.9	0.9	-1.2	-5.1	0.0	-3.5
		2	0.8	0.9	-0.5	-2.5	1.3	0.0
PLUTO2	200	1	0.5	0.7	-0.4	-1.8	1.4	0.5
		2	0.5	0.7	-0.4	-1.6	1.6	0.6
EPIC	600	2	1.0	0.9	-2.1	-7.1	0.5	-3.4

2. Discussion of Pin Failure Pressure in Slow TOP Accidents (H. H. Hummel and P. A. Pizzica)

According to the clad strength data we are using, which are based on the DiMelfi-Kramer fuel adjacency effect theory[5], the pin pressure at the clad wall required to produce failure for the clad temperature prevailing when a maximum melt fraction of 0.50 is attained is about 130 atm at the top of the core and about 300 atm at the core midplane.

For a cavity model with strengthless fuel the pressure at the clad wall is reduced from the cavity pressure by the ratio of the cavity radius to the clad inner radius. This would give a cavity pressure to produce failure of about 400 atm for a midplane failure at 0.50 fuel melt fraction. Therefore a pressure this high at 0.50 fuel melt fraction is possible with a cavity model.

Pin pressure in EPIC at clad failure time was adjusted by varying gas volume, as we have no reliable way to calculate this volume. At 0.50 melt fraction, with gas pressure averaged over entire pin in the core (non-cavity

model), the FRESS module of SAS/EPIC calculated a pre-failure gas pressure of 185 atm based on a void fraction of 0.092, which is in a reasonable range. For this model, which seems more realistic than the cavity model for a slow TOP, failure by gas pressure will be near the top of the core at a relatively low pressure. This will not lead to immediate molten fuel ejection but will reduce the gas pressure prevailing at the time of molten fuel ejection resulting from a midplane failure. Early clad failure from differential expansion should also lead to gas evolution prior to molten fuel ejection. These considerations make it appear more likely that the pin failure pressure for a slow TOP will be in the range 100-200 atm rather than higher, say 400-600 atm.

3. Results of EOC-3 TOP Calculations for the CRBR with a Pin Enthalpy Failure Criterion (P. A. Pizzica and H. H. Hummel)

In TOP calculations for the CRBR EOC-3 core with SAS3D/EPIC reported in the previous quarterly[6], a large degree of failure coherence was found for reactivity ramp rates of 10 ¢/sec or greater. It is now realized that this tendency was accentuated by certain aspects of the steady-state fuels characterization calculations combined with an assumed fuel melt fraction failure criterion and the assumed radial structure in the SAS3D/EPIC calculations. For a higher steady-state power, more columnar fuel is formed, which would normally lead to a higher fuel density in the inner part of the pin. However, the GE swelling correlation used in these calculations gives a high swelling rate with burnup for a columnar fuel, actually yielding a lower density than for equiaxed and unrestructured fuel. The net result of this is that, because the average fuel melt fraction is defined on a mass-averaged basis and because the radial mesh structure is fairly coarse, it is possible at times for the calculated melt fraction increase for a given increase in pin enthalpy to be less for higher power fuel than for lower power because there is more fuel mass in the outer part of the pin that has not yet reached the solidus and whose added heat content therefore does not increase the calculated melt fraction. This turned out to be an important effect in increasing failure coherence in the EOC-3 calculations. Also, there were "plateaus" in the time dependence of fuel melt fraction in which the value did not change for a considerable time. These effects are artifacts of the calculation rather than real physical phenomena, and it was found possible to eliminate them by using a failure criterion of attainment of pin enthalpy corresponding to 0.50 melt fraction.

For the new calculations, the failure coherence as expressed by the times between failure of the lead channel 10 and of channel 11, next to fail, is as follows:

Ramp Rate, ¢/s	Time, Milliseconds
10	60
20	25
50	15

The 60 msec separation in failure time between channels 10 and 11 obtained with SAS/EPIC at 10 ¢/sec is of the same order as that found with SAS4A. Based on these results, it is concluded that for ramp rates of 10 ¢/sec or less development of an autocatalytic situation seems unlikely even with

weak sweepout developing over 20-40 milliseconds and an assumed core midplane failure. For a ramp rate of 20 ¢/sec, SAS/EPIC calculations indicate autocatalytic conditions are being approached with a core midplane failure for a relatively weak sweepout corresponding to 100 atm failure pressure and a mild FCI. There may be even more potential for autocatalysis at 20 ¢/sec when using PLUTO2 in SAS4A because of somewhat weaker sweepout. Autocatalysis would become quite severe at 50 ¢/s, although we have not rerun such cases with an enthalpy failure criterion.

B. BIFLO Code Development (P. L. Garner)

1. Modeling Changes

A procedure has been developed to semiautomatically adjust the array sizes in BIFLO (prior to compilation) to the minimum required for a particular problem. This provides the flexibility to consider many different problem geometries and reduces the overall computing costs.

The boundary condition at the fuel assembly inlet for the axial momentum equation is now an input-selectable option: either pressure or velocity may be specified. Specification of pressure, which was the original boundary condition in BIFLO, is still the preference for most problems of interest. The availability of the velocity boundary condition allows examination of inlet flow blockage cases and comparisons with other codes which have only a velocity boundary condition.

2. Loss-of-Flow Calculations for Various Bundle Sizes

Calculations have been performed using BIFLO to examine multidimensional aspects of sodium boiling for several bundle sizes as a follow-on to the pretest calculations[7] performed for the 15-pin OPERA Facility experiment. The additional calculations have examined full hexagonal bundles containing 37, 61, and 217 pins. The calculations used the same basic dimensions (e.g. pin diameter, pin-to-pin spacing, and heated length), "fuel" properties, and boundary conditions (e.g. power per pin, inlet temperature, inlet and outlet pressure histories) as were used for the pretest calculations of the 15-pin OPERA Facility experiment. As a small variance from this, the 37-pin bundle had a gap between the outer pin row and the can wall of one-half the pin-to-pin gap in order to simulate the geometry of the P3A and P3 tests run in the Sodium Loop Safety Facility. For most of the two-dimensional calculations, each of the outer three physical coolant rings in the bundle was a separate BIFLO channel, and the remainder of the bundle interior formed the fourth BIFLO channel. One-dimensional calculations of these bundles were also performed.

A summary of the results for these calculations is shown in Table III. Calculated results for the 217-pin hexagonal bundle are similar to those shown previously[6] for the 15-pin OPERA Facility experiment: a two-dimensional analysis predicts that inlet flow reversal will occur earlier than would be calculated using a one-dimensional analysis. In contrast, there is essentially no difference between the timings of inlet flow reversal calculated with one- and two-dimensional models for the 37- and 61-pin bundles. For all cases, the time elapsed between sustained boiling across the entire bundle flow area and inlet flow reversal in the two-dimensional calculations is less than (by 13

TABLE III. Timing[a] (seconds) of Characteristic Events Calculated Using BIFLO

Number of Pins	37	61	15	217
Geometry	hexagonal	hexagonal	triangular	hexagonal
Pin-to-wall gap / Pin-to-pin gap	0.5	1.0	1.0	1.0
One-Dimensional Calculations:				
Initial Boiling	9.0 (0)	11.45 (0)	11.70 (0)	9.65 (0)
Inlet Flow Reversal	9.57 (0.57)	11.92 (0.47)	12.25 (0.55)	10.15 (0.50)
Two-Dimensional Calculations:				
Initial Boiling	8.0 (0)	7.15 (0)	6.35 (0)	7.25 (0)
Sustained Boiling Across Entire Bundle Flow Area	9.10 (1.10) [0]	11.52 (4.37) [0]	10.87 (4.52) [0]	8.87 (1.62) [0]
Inlet Flow Reversal	9.55 (1.55) [0.44]	11.93 (4.78) [0.41]	11.34 (4.99) [0.47]	9.26 (2.01) [0.39]

[a]The normal entries in the table are time relative to initiation of the flow coastdown.
() - denotes time elapsed since initial boiling.
[] - denotes time elapsed since sustained boiling occurred across entire bundle flow area.

to 22%) the time elapsed between boiling initiation and inlet flow reversal in the one-dimensional calculations. The statement in Ref. 7 that these times were identical for the 15-pin bundle calculations was incorrect; a re-examination of the calculated results revealed that sustained boiling occurred later than the time reported.

The dividing line between one- and two-dimensional behaviors is a function of more than just the physical bundle size, as evidenced by the difference in behaviors calculated for the 61-pin hexagonal bundle and the 15-pin triangular bundle which are similar in "radial" dimension. The distribution of power-to-flow ratio across the bundle, which is different for the 61-pin and 15-bundles, appears to be an additional important factor. The results of these cases are being examined further to try to quantify the conditions under which a two-dimensional calculation is required for analysis of boiling through the time of inlet flow reversal.

3. Inlet Flow Blockage for CRBR

In response to a request from the NRC CRBR Project Office, work has been initiated to examine the impact of two-dimensional boiling modeling on analysis of the sudden total blockage of the inlet flow area of a CRBR fuel assembly. The data needed to characterize a fuel assembly (e.g. geometry, hydraulics, power distribution, and material properties) have been extracted for the lead channel from a SAS3D/EPIC calculation at EOC-4 conditions. As a check on the preparation of the fuel assembly characterization, the results calculated using this input and a one-dimensional modeling in BIFLO were found to be in good agreement with those calculated by SAS3D/EPIC for the first 8 s of the reference loss-of-flow accident sequence.

Attention was then directed toward examining the inlet flow area blockage case. The flow cannot be changed instantaneously from full flow to zero flow because this rapid deceleration would be associated with an unphysical pressure profile in the assembly. A finite period of time would probably be required for a flow blockage to actually occur. The inlet flow area blockage

has been simulated in BIFLO by decreasing the inlet velocity linearly to zero over a specified period of time, from $t=0$ to $t=t_{block}$. A series of BIFLO calculations has been performed for various values of t_{block} less than 1 s. The absolute timings of events in BIFLO were found to be a function of t_{block}; however, the timings of events when measured relative to the time of initial sustained boiling are not a strong function of t_{block}. In the limit as t_{block} approaches zero, the boiling initiation time appears to be limiting to 1.44 s for a one-dimensional case and 0.98 s for a two-dimensional case.

Boiling initiates near the axial centerplane of the core for the inlet flow blockage cases, rather than the top-of-core boiling associated with the reference loss-of-flow calculation. The net upward voiding during the first 0.25 s following boiling initiation is about the same in the one- and two-dimensional cases. Voiding progresses downward somewhat more rapidly in the two-dimensional case than in the one-dimensional case. After ~0.25 s, the upper half of the core is highly voided in the one-dimensional case; the voiding in the two-dimensional case extends somewhat further axially at this time but sustained boiling adjacent to the fuel assembly wall has not begun.

The two-dimensional cases are running too slowly for extended comparisons between one- and two-dimensional behaviors to be made at this time. This is due primarily to an inadequate treatment of highly voided (including pure vapor) cells in BIFLO. Additionally, the lateral conduction of heat from channel to channel, which is currently not modeled in BIFLO, appears to be an important term during the calculation for $t>t_{block}$ since the axial flow and lateral crossflow are small. The methods needed to improve the calculation in these two areas are being developed for implementation.

II. THREE-DIMENSIONAL CODE DEVELOPMENT FOR CORE THERMAL-HYDRAULIC ANALYSIS OF LMFBR ACCIDENTS UNDER NATURAL CONVECTION CONDITIONS

A2045

A. Introduction

The objective of this program is to develop computer programs (COMMIX and BODYFIT) which can be used for either single-phase or two-phase thermal-hydraulic analysis of reactor components under normal and off-normal operating conditions, especially under natural circulation. The governing equations of conservation of mass, momentum, and energy are solved as a boundary value problem in space and an initial value problem in time.

COMMIX is a three-dimensional, transient, compressible flow computer code for reactor thermal-hydraulic analysis. It is a component code and uses a porous medium formulation to permit analysis of a reactor component/multicomponent system such as fuel assembly/assemblies, plenum, piping system, etc., or any combination of these components. The concept of volume porosity, surface permeability, and distributed resistance and heat source (or sink) is employed in the COMMIX code for quasi-continuum (or rod-bundle) thermal-hydraulic analysis. It provides a greater range of applicability and an improved accuracy than subchannel analysis. By setting volume porosity and surface permeability equal to unity, and resistance equal to zero, the COMMIX code can equally handle continuum problems (reactor inlet or outlet plenum, etc.).

BODYFIT is a three-dimensional, transient, compressible flow computer code for reactor rod bundle thermal-hydraulic analysis. BODYFIT is a component code and uses a boundary-fitted coordinate transformation technique. The complex rod bundle geometry is transformed into either rectangular or cylindrical coordinates with uniform mesh. Thus, the physical boundaries, including each rod, coincide with computational grids. This allows the Navier-Stokes equations, together with the boundary conditions, to be represented accurately in the finite-difference formulation. Thus, the region in the immediate vicinity of solid surfaces, which is generally dominant in determining the character of the flow, can be accurately resolved.

B. COMMIX-1A, Single-Phase Code Development (W. L. Baumann, F. F. Chen, H. M. Domanus, J. R. Hull, R. C. Schmitt, W. T. Sha, J. E. Sullivan and S. P. Vanka)

B.1 Development Work

During this quarter, primary efforts were spent towards documentation of the COMMIX-1A code. Most sections of the report are written and they are being typed. Simultaneously, (i) as a benchmark test, the problem "Flow Through a Hexagonal Fuel Assembly with Planar Blockage" was rerun, (ii) several errors detected during analysis were corrected, (iii) water property package was implemented, and (iv) a separate graphic package for geometry with irregular boundaries was prepared.

Turbulence Model

The (k-ε) two-equation model has been formulated and implemented in the code. Here, k is the kinetic energy of turbulence, and ε is the dissipation rate of kinetic energy. In this model, two partial differential equations one for k, and the other for ε, are solved. The local effective viscosity which is now a function of k and ε, is then calculated and used in the solution of momentum equations.

In order to ensure that the model is properly implemented and that there are no programmatic errors, the following two problems were simulated.

(i) Developing Turbulent Flow in A Pipe (Re_{in} = 388,000)

A uniform finite-difference grid of 20 x 50 nodes in the r and z directions was used. The inlet kinetic energy was prescribed to be $0.001\ w^2$, and the inlet dissipation rate of kinetic energy to be $C_\mu k^{3/2}/(.03L)$ where L was taken to be the radius of the outlet. Figure 5 presents the velocity profiles at four axial locations along the pipe. When compared with experimental data of Ref. 8, we observe very good agreement at large z, but some discrepancy is seen at the inlet z locations. The discrepancy is probably due to errors in the prescription of the inlet dissipation rate (no measurements are available).

(ii) Axisymmetric Sudden Expansion (Radius ratio = 2; $Re \sim 2\times10^5$)

For this problem, Ref. 9, a 10 x 50 finite-difference grid was employed. The inlet k was taken to be $0.001\ w^2$ and the inlet dissipation rate of kinetic energy to be $C_\mu k^{3/2}/0.03r_i$. Figures 6 and 7 present the profiles of velocity and $\sqrt{2/3}\ k/w$ at three axial locations. As can be seen, the agreement is satisfactory in both the velocities and the kinetic energies. The small discrepancies in velocities have been observed in earlier studies, also Ref. 10. They are due to errors in the (k-ε) model.

B.2 Validation of COMMIX-1A for Preparation of CRBR Licensing

FFTF Simulation

The steady-state and transient simulations of FFTF in-vessel thermal hydraulics have been completed. The numerical results, modeling and comparison of results for the steady-state case are presented in the report "COMMIX-1A Three-Dimensional In-Vessel Simulation of the FFTF Thermal Hydraulics," NUREG/CR-2535, ANL-CT-82-1 (Jan 1982).

The transient simulation is a case of flow coast-down from full flow to natural circulation in combination with a reactor scram from full power. The numerical modeling, solution procedure, and comparison of results are presented in the report "COMMIX-1A Three-Dimensional In-Vessel Simulation of the FFTF Transient Thermal Hydraulics," by S. P. Vanka, H. M. Domanus, and W. T. Sha, NUREG/CR-2773, ANL-CT-82-14 (May 1982).

Following is a summary of the results and conclusions:

The geometrical details and the flow conditions pertinent to this simulation are given in the Appendix A. Figures 8(a) and (b) show the finite-difference grid employed. In order to reduce the computer time required, a 120° sector of the vessel was simulated. Figures 9 and 10 show the calculated steady-state flow pattern and the isotherms at two selected (r-z) planes. Figures 11(a-c) show the transient function of flow and power employed in the present simulation. Figures 12-14 show the flow patterns at time t = 29, 53, and 79 secs., and Figs. 15-17 show the temperature contours for the same times.

The important observations from this study are the complex flow and temperature patterns during the transient, and the thermal stratification in the upper plenum. It is seen that the hot fluid is trapped in the top portion of the plenum, and the cold fluid (after the power shutdown) by-passes the hot fluid, flowing directly from the core exit to the outlet. Because of this flow condition, the thermal liner of the vessel wall is subjected to a large temperature gradient. We also observe that the flow from the core is strongly coupled with the thermal hydraulics of the upper plenum.

The results of the calculations have been compared with the measured data. The quantities compared are the exit temperatures and flows from the fuel and reflector assemblies, the temperatures in the upper plenum as measured by the Temperature and Liquid Level Monitors (TLLMs), and the temperature at the Proximity Test Plug (PTP). Figure 18 shows the FOTA exit temperature with time and Figure 19 shows the calculated TLLM temperature near the outlet nozzle. Figure 20 shows the calculated PTP temperature compared with data. It is seen that except in the immediate period following the transient, the agreement between calculations and measurements are satisfactory.

EBR-II Simulation

A two-dimensional in-vessel thermal-hydraulic simulation of the EBR-II Pool Reactor Transient Test No. 10, Phase 2, has been completed. The simulation was performed using the implicit formulation of the COMMIX-1A computer code.

The numerical modeling, solution procedure, computational results and comparison with experimental data for steady-state and a 200-s transient are presented in the report "EBR-II In-Vessel Natural Circulation Analysis," by W. L. Baumann, H. M. Domanus, D. Mohr, R. C. Schmitt, J. E. Sullivan, and W. T. Sha, NUREG/CR-2821, ANL-CT-82-19 (June 1982).

Following is a summary of simulation and results.

In the present simulation, a two-dimensional approach was taken using a grid system of 24 axial x 14 radial cells (see Fig. 21). The geometric and operating characteristics are presented in the Appendix B. The main components to be modeled were the subassemblies including driver, reflector and blanket region, the lower plena (high-pressure and low-pressure plenum), the upper plenum, inlet pipe and outlet pipe. Two basic flowpaths separating at the inlet of the configuration were simulated: high-pressure

flow feeding into high-pressure plenum and driver region, and low pressure flow feeding into low pressure plenum, reflector and blanket region. A junction between both flowpaths established at the boundary surface of the two inlet cells allowed for a general flow redistribution during a transient.

Two transient functions were employed for the simulation, (i) a severe flow transient reducing the total reactor inlet mass flow from 100% nominal value to less than 1% within 45 s, and (ii) a minor power transient initiated at about 1.5% of nominal power generation and following the law of decay.

The steady-state results show both high-pressure and low-pressure flow entering the lower plena and moving up through the subassemblies (Fig 21).

Reversed flow in the low pressure plenum observed during a short time interval of the EBR-II test has been confirmed by the transient calculation (Fig. 22). Comparisons of temperatures and mass flow rates indicate a close agreement between simulation and experiment.

Figure 23a shows a comparison between COMMIX-1A and measured EBR-II transient data for the top of core thermocouple of the driver subassembly XX08. Figure 23b shows a comparison for the low-pressure plenum flow where reversed flow is clearly seen to occur between 50 and 150 seconds.

Encouraged by these results, we are now performing a three-dimensional simulation to obtain more detailed results. The input data preparation for the 3-D case has been initiated.

CRBR Primary Vessel

The preliminary modeling of CRBR primary vessel for numerical simulation with COMMIX-1A has been completed. A steady-state solution has been achieved for full-power full-flow conditions. A sample velocity distribution of the solution is shown in Fig. 24, and a sample temperature distribution of the solution is shown in Fig. 25.

A report describing the modeling of the CRBR primary vessel has been written. This is to elicit comments from the nuclear community so that the model can be improved to more accurately reflect the critical features of the CRBR primary vessel.

C. COMMIX-2, Two-Phase Code Development (H. M. Domanus, C. C. Miao, W. T. Sha, and V. L. Shah)

During this quarter, the resimulation of the German seven-pin transient confirmed that modifications and improvements have not introduced any errors. The simulation was continued and a converged solution up to a transient time of t = 10.32 sec. has been obtained. Some difficulty has been observed at the transient time of t = 10.34 sec. when one of the computational cells in the boiling region has superheated vapor. We are now looking into this problem.

D. BODYFIT Code Development (B. C-J. Chen, I. Eldib, and W. T. Sha)

To further test the applicability of the new pressure-correction scheme described in the last quarterly report, the problem "Flow in a 90°-Bend Elbow" was resimulated. The geometry and the boundary conditions used for the simulation correspond to the experimental work of Murakami.[11] They are:

Pipe radius : 0.0538 m

Reynolds number : 10^5

Inlet velocity : 182 m/s

For simplicity in calculation and to save computer running time, the turbulent viscosity was evaluated from the equation:

$$\mu_t = 0.007\ C_\mu \rho u_{max} \ell \ .$$

We used the following values

$C_\mu = 0.1$,

$\ell = 0.4\ D_h$,

$U_{max} = 1.82$, and

$\rho = 998\ kg/m^3$

to arrive at $\mu_t = 27\ \mu_\ell$.

The results of the simulation are shown in Figs. 26-28. The axial velocity in the bend plane is shown in Fig. 26. The comparisons of axial and swirling velocity at line E-E are shown in Figs. 27-28.

The efforts in the coming months will be devoted to debugging and testing of the one-equation (k) and two-equation (k-ε) turbulence models implemented in BODYFIT-1FE.

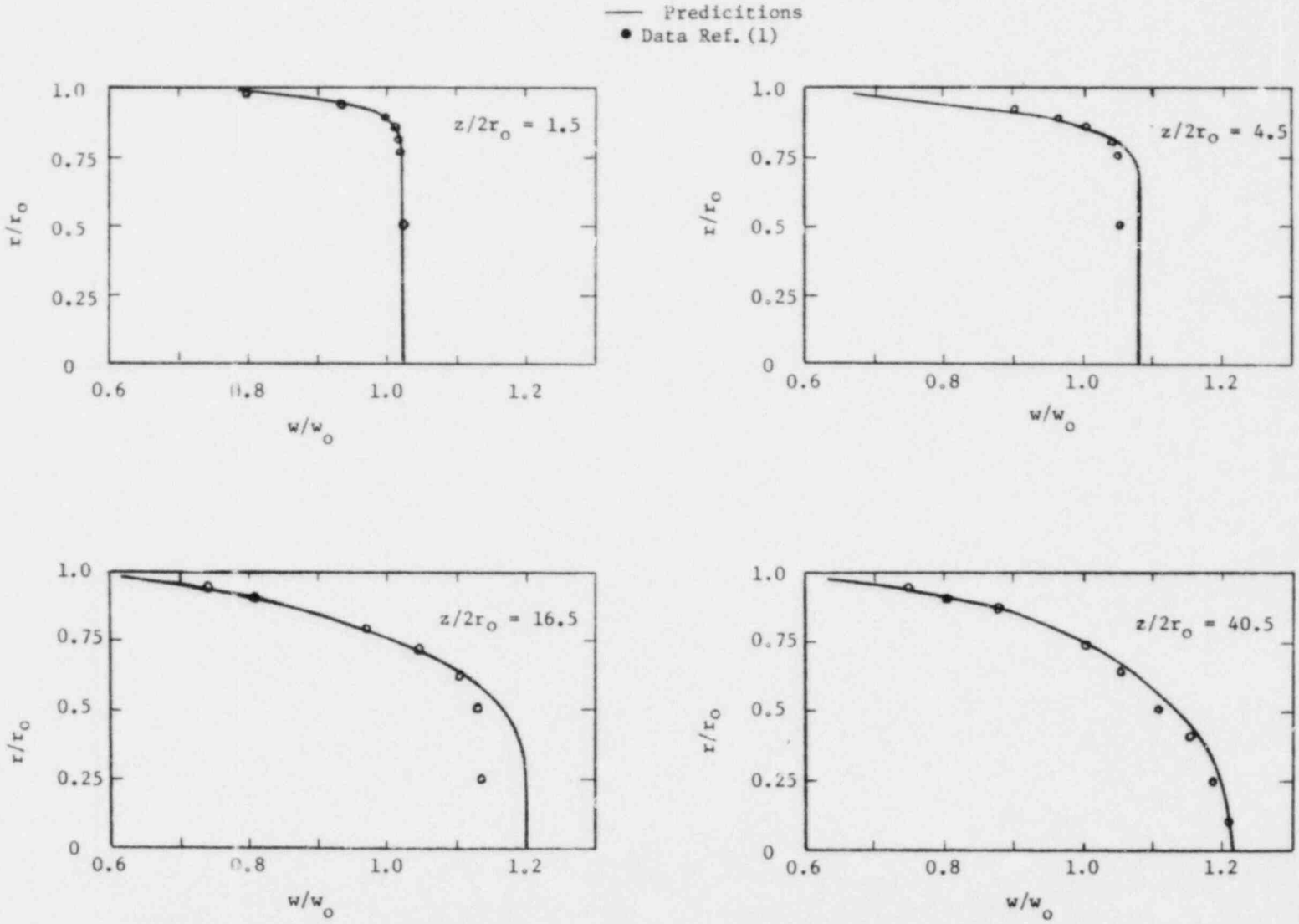

Fig. 5. Development of Axial Velocity Profiles at Various Distances in a Straight Pipe

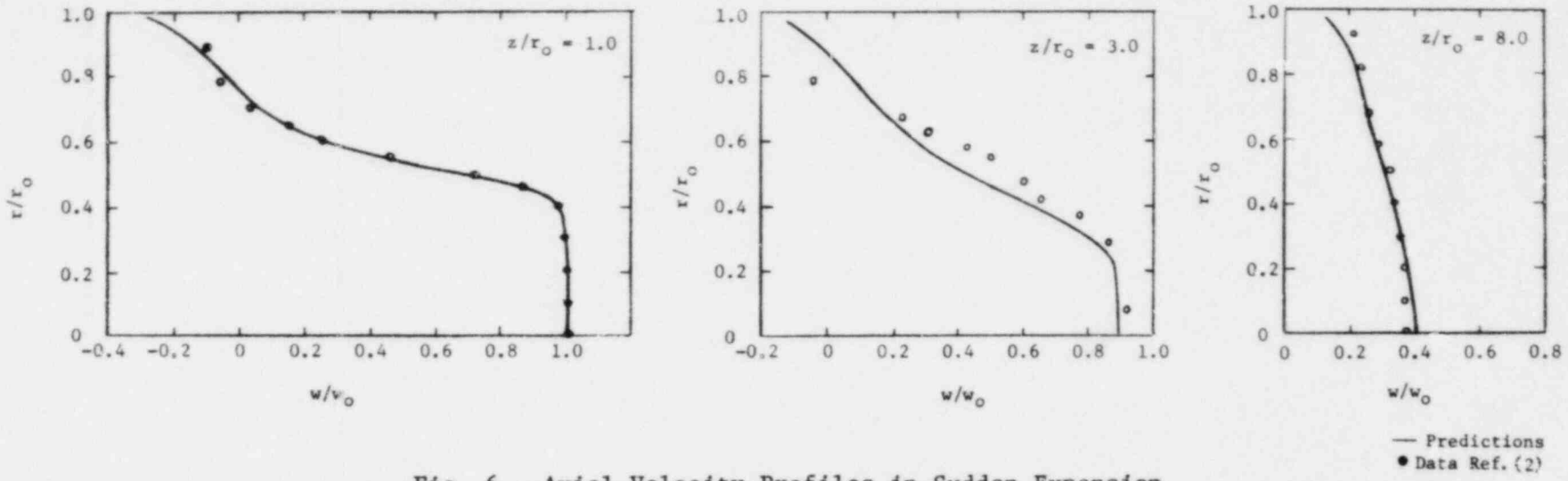

Fig. 6. Axial Velocity Profiles in Sudden Expansion

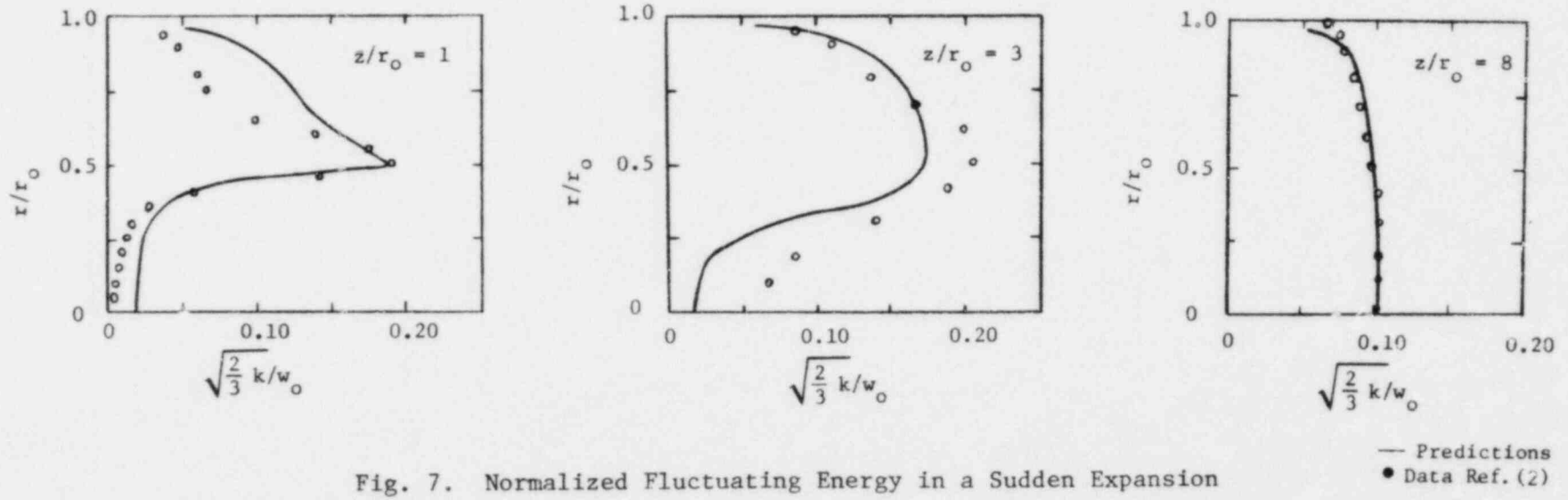

Fig. 7. Normalized Fluctuating Energy in a Sudden Expansion

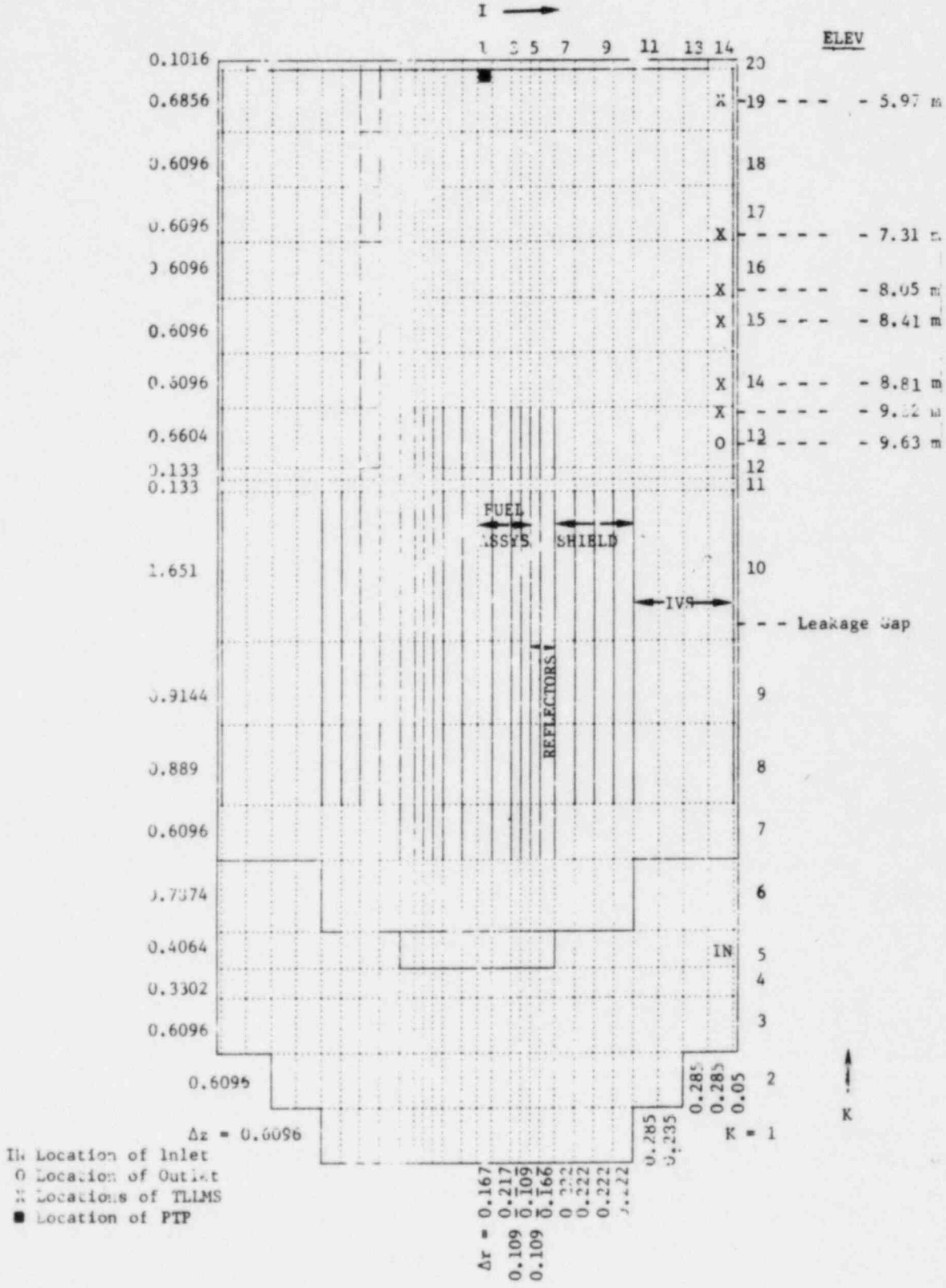

Fig. 8a. Finite-difference Grid in R-Z Plane

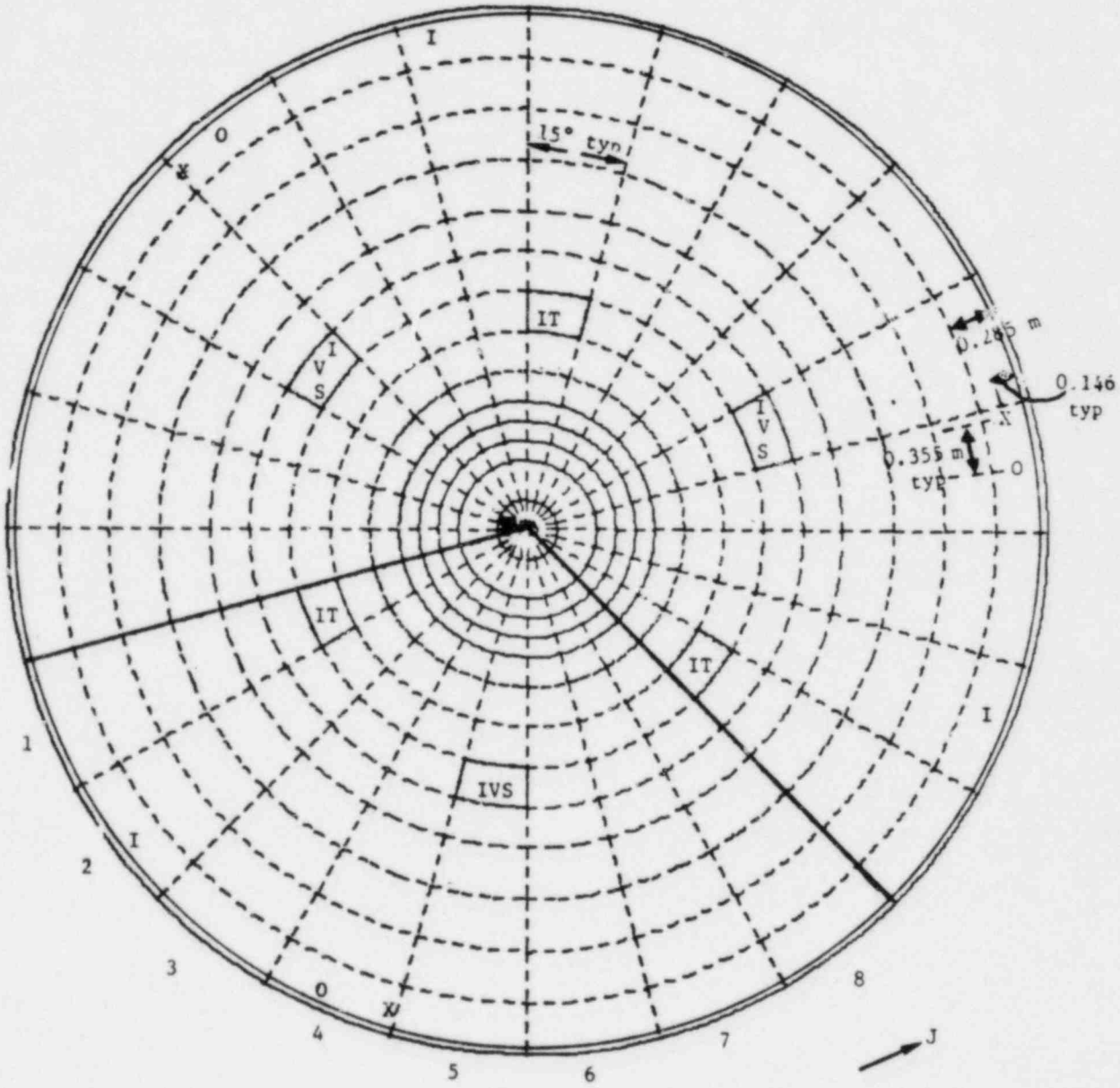

O Locations of Outlets

I Locations of Inlets

X Locations of TLLMs

■ Location of PTP (above fuel assembly 2202)

Fig. 8b. Finite-difference Grid in R-θ Plane

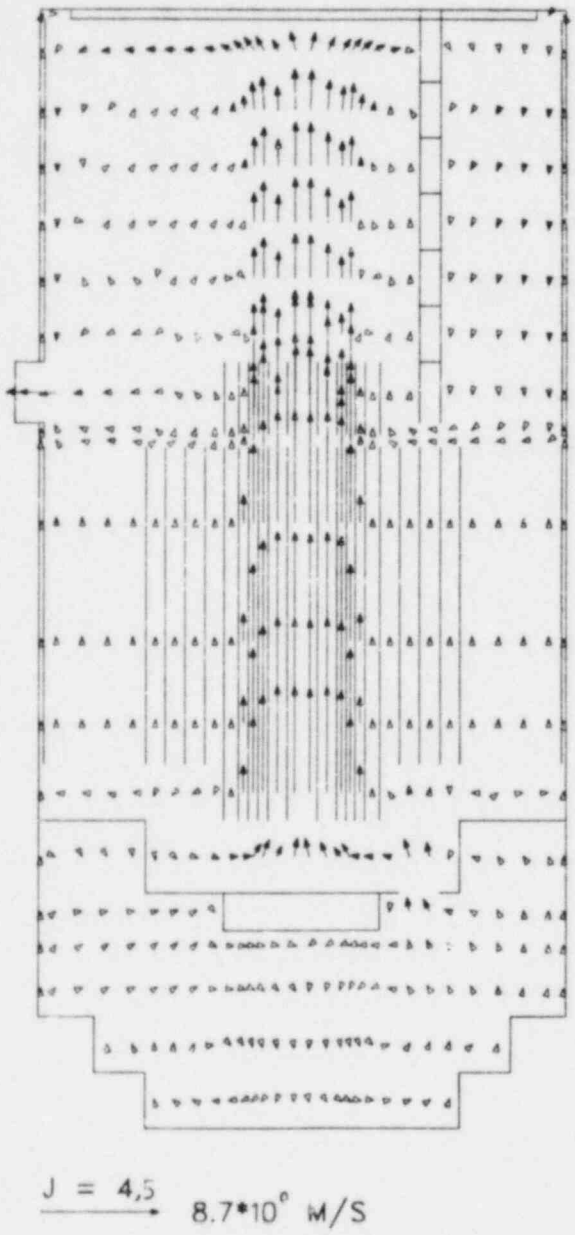

Fig. 9. Velocity Vectors in the R-Z Plane at Steady State

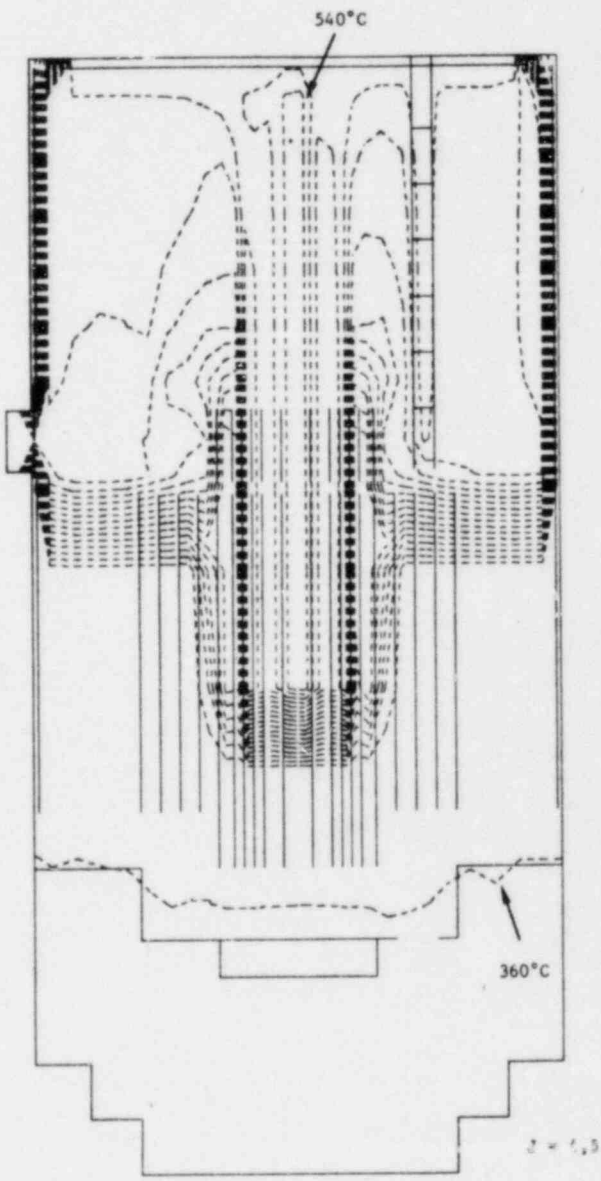

Fig. 10. Contours of Equal Temperature at Steady State ($\Delta T = 10°C$)

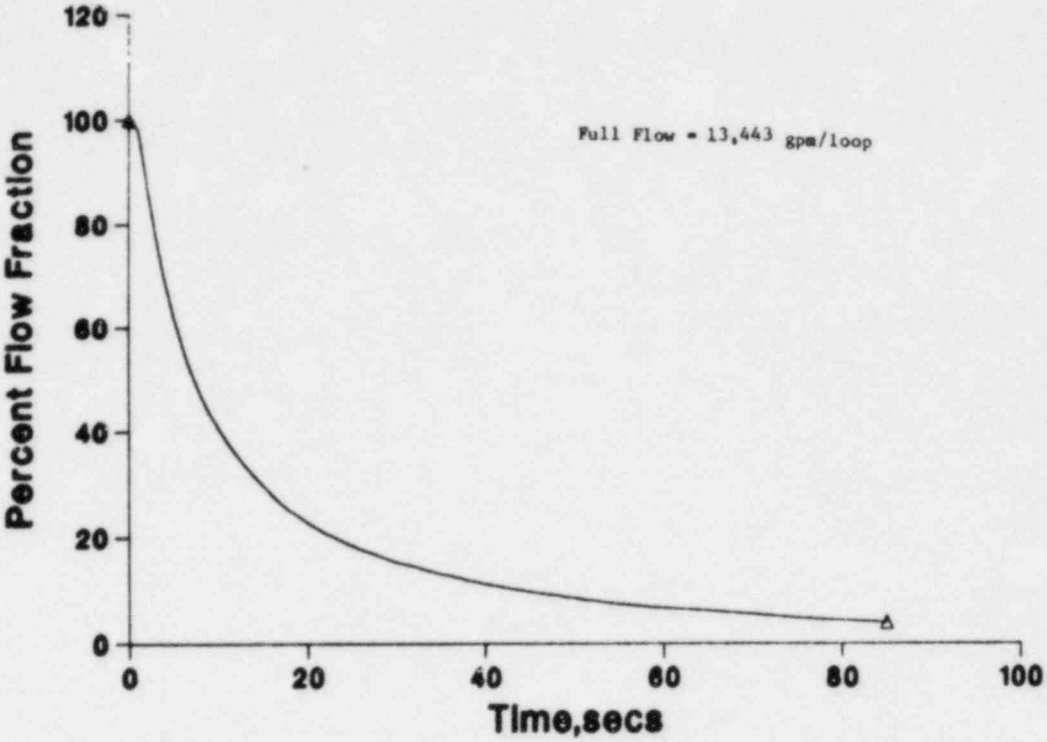

Fig. 11a. Transient Flow Function

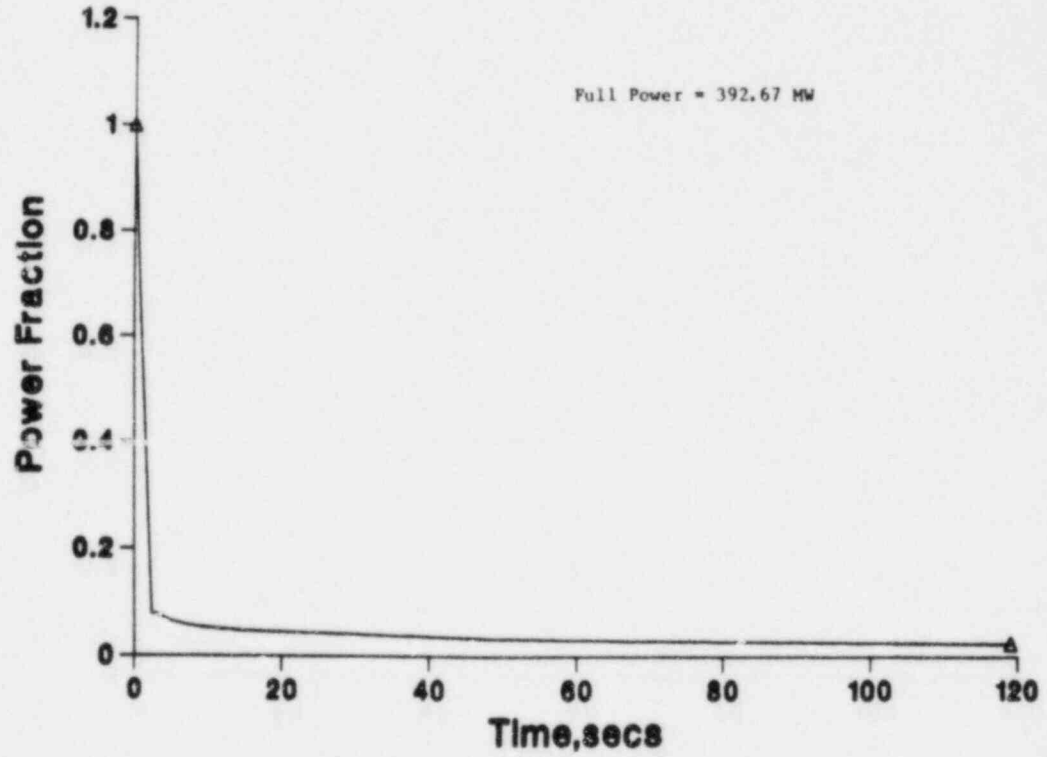

Fig. 11b. Core Power Function

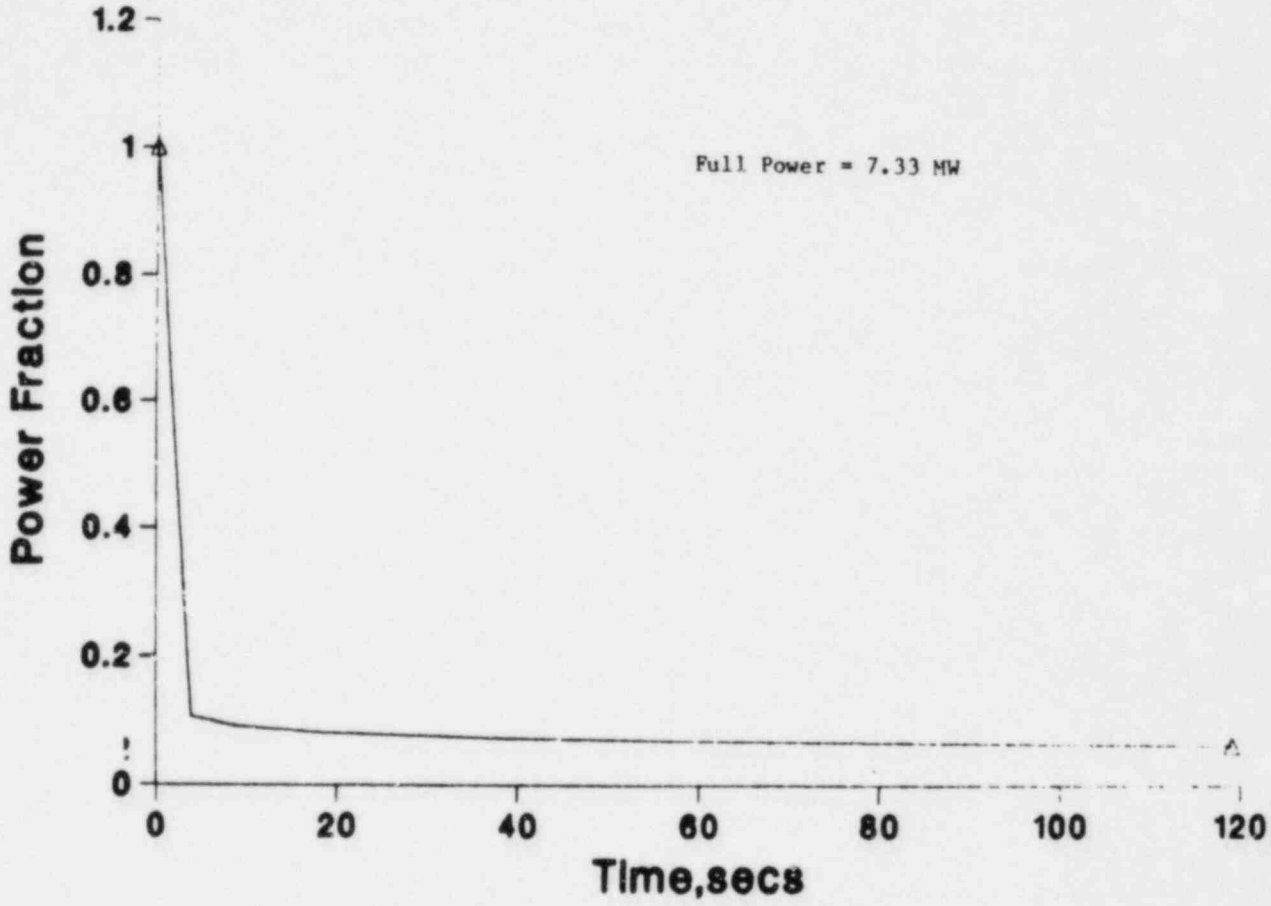

Fig. 11c. Reflector Power Function

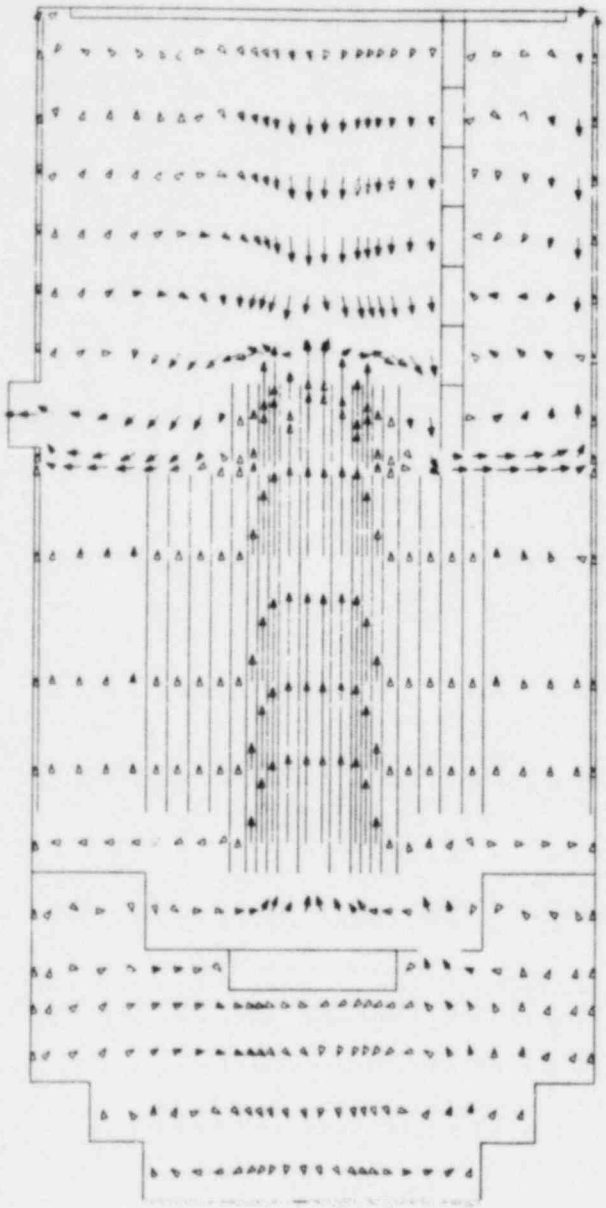

Fig. 12. Velocity Vectors at t = 29 sec

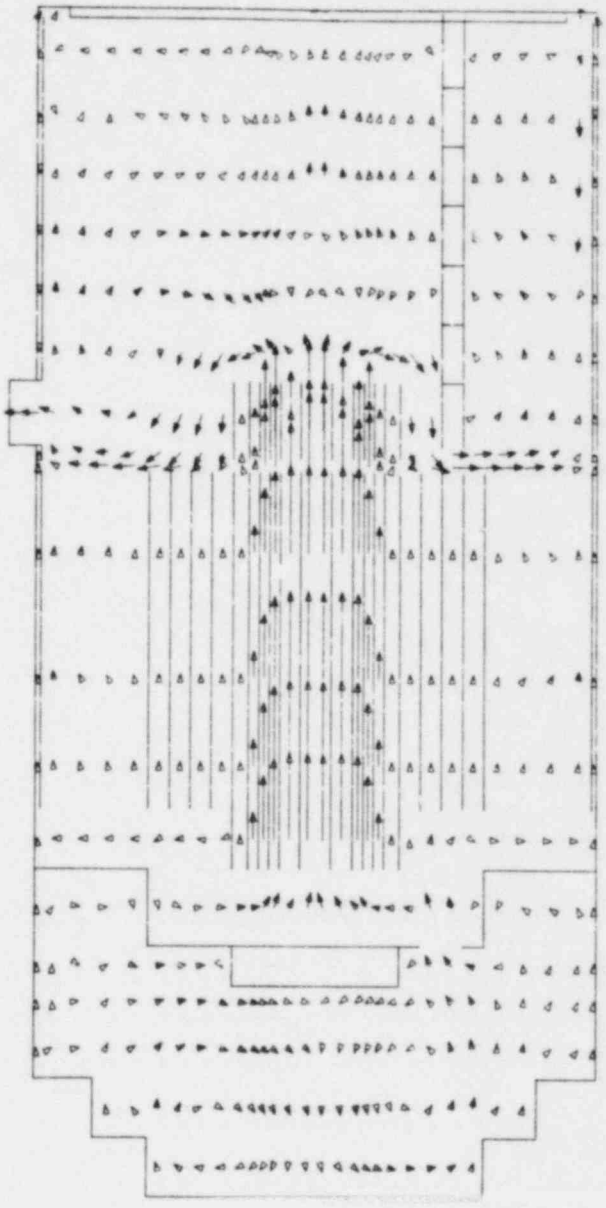

Fig. 13. Velocity Vectors in R-Z Plane at t = 53 sec

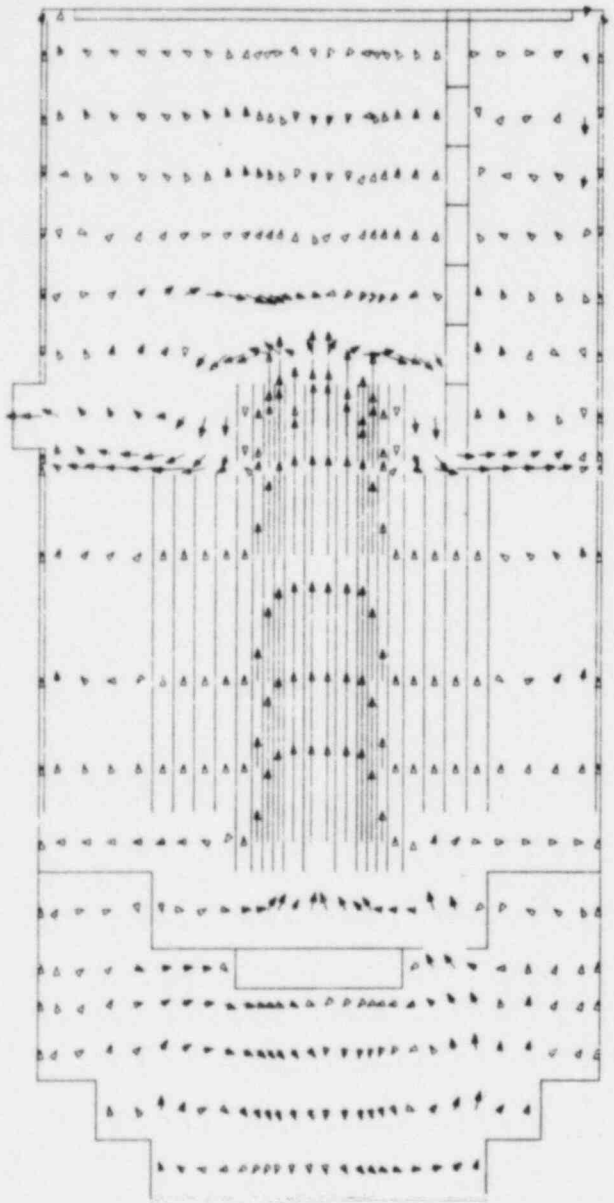

Fig. 14. Velocity Vectors in R-Z Plane at t = 79 sec

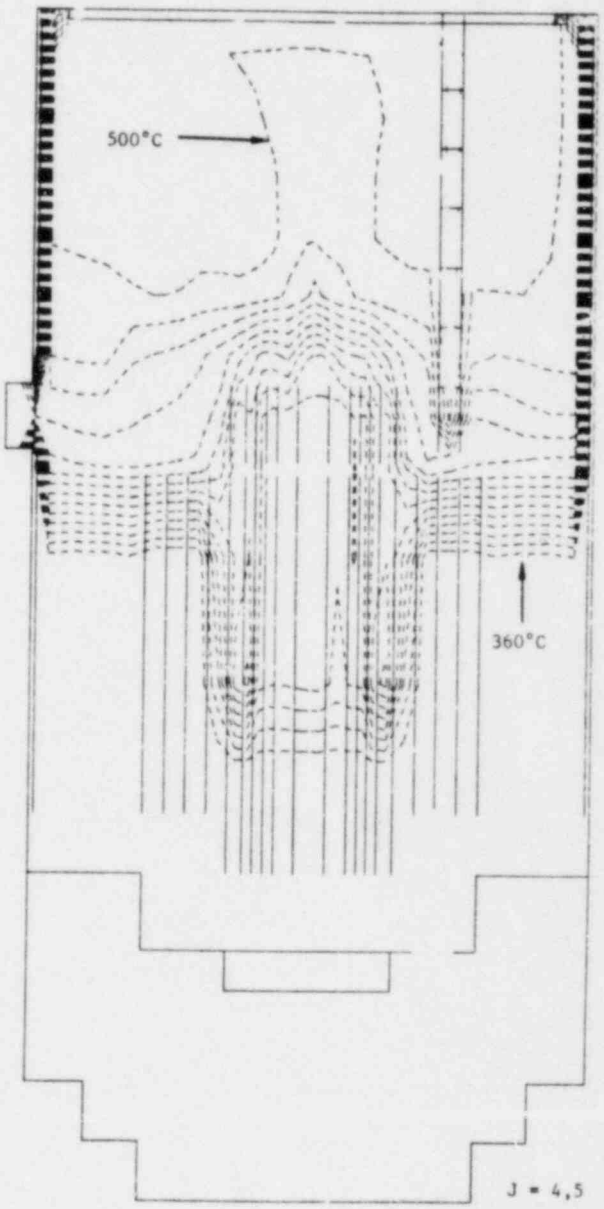

Fig. 15. Temperature Contours at t = 29 sec (ΔT = 10°C)

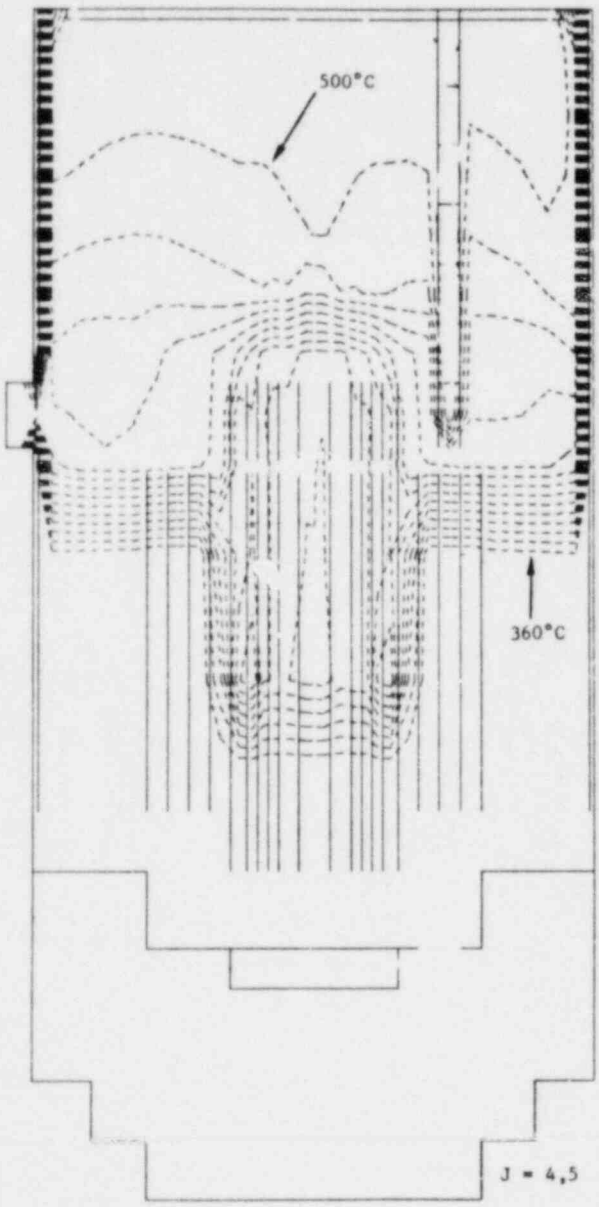

Fig. 16. Temperature Contours at t = 53 sec (ΔT = 10°C)

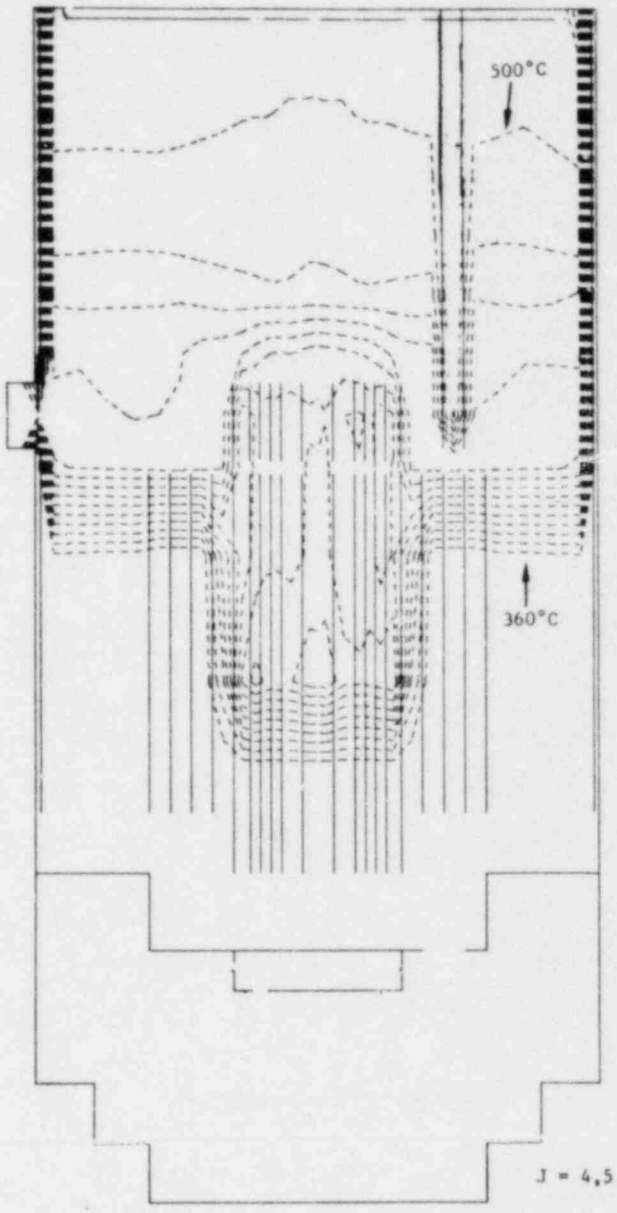

Fig. 17. Temperature Contours at t = 79 sec (ΔT = 10°C)

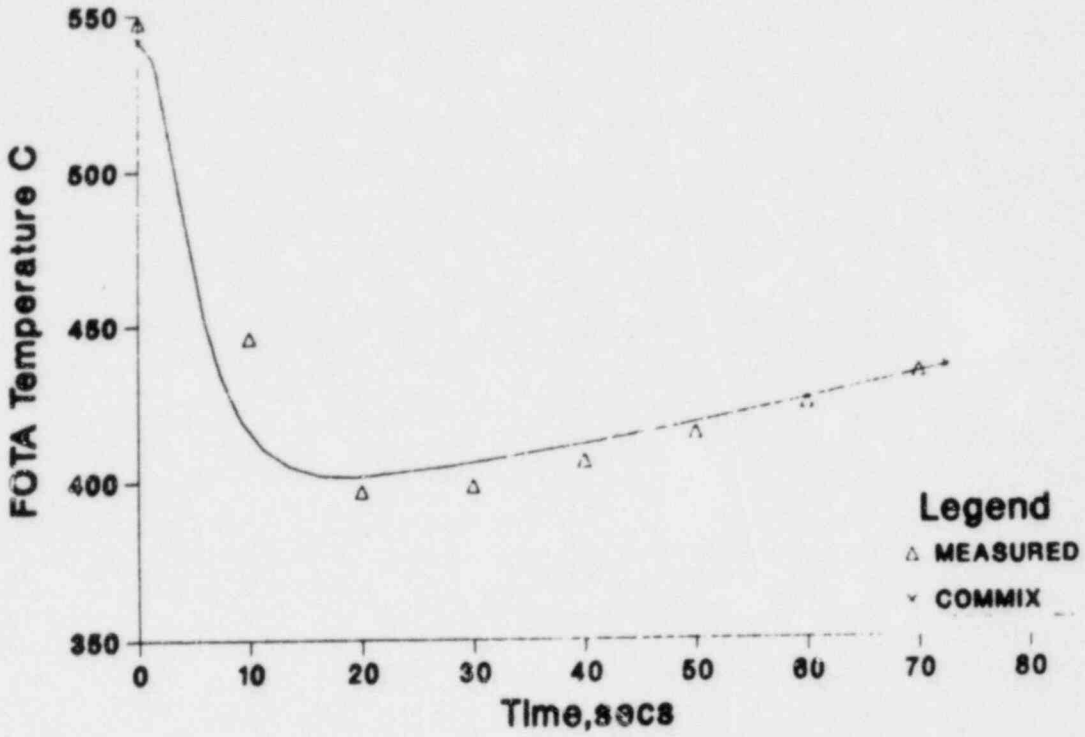

Fig. 18. Comparison of (Row 2) FOTA Exit Temperature

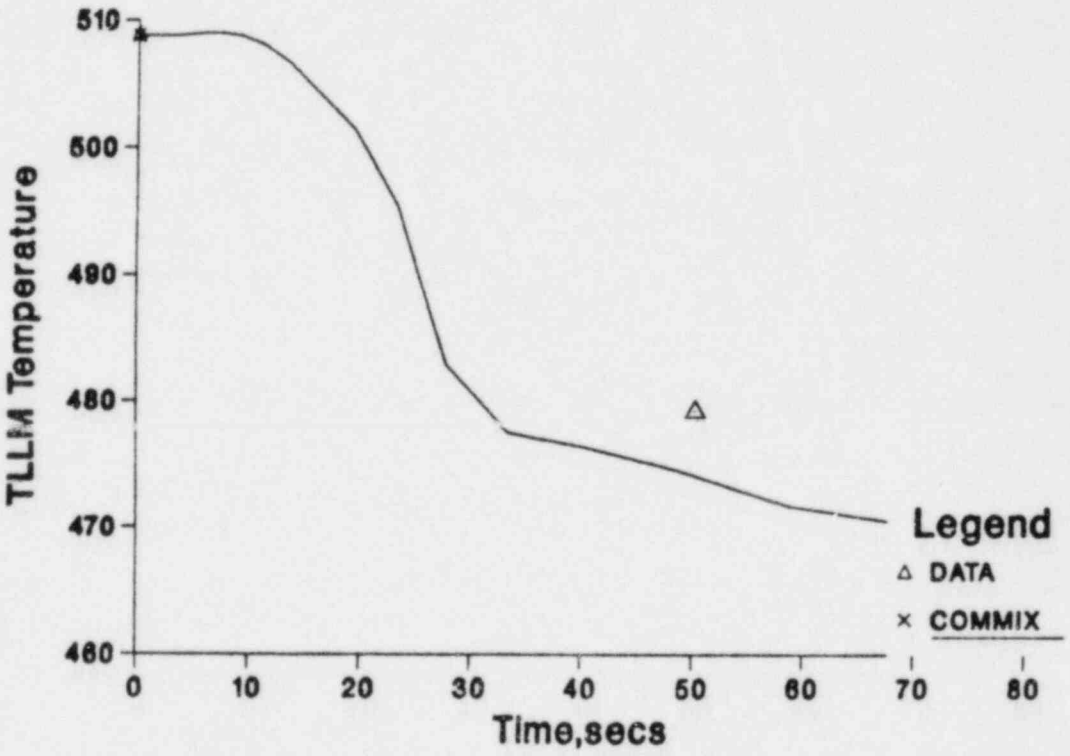

Fig. 19. Comparison of Calculated and Measured TLLM Temperatures at Elevation -30'7" (-9.32 m)

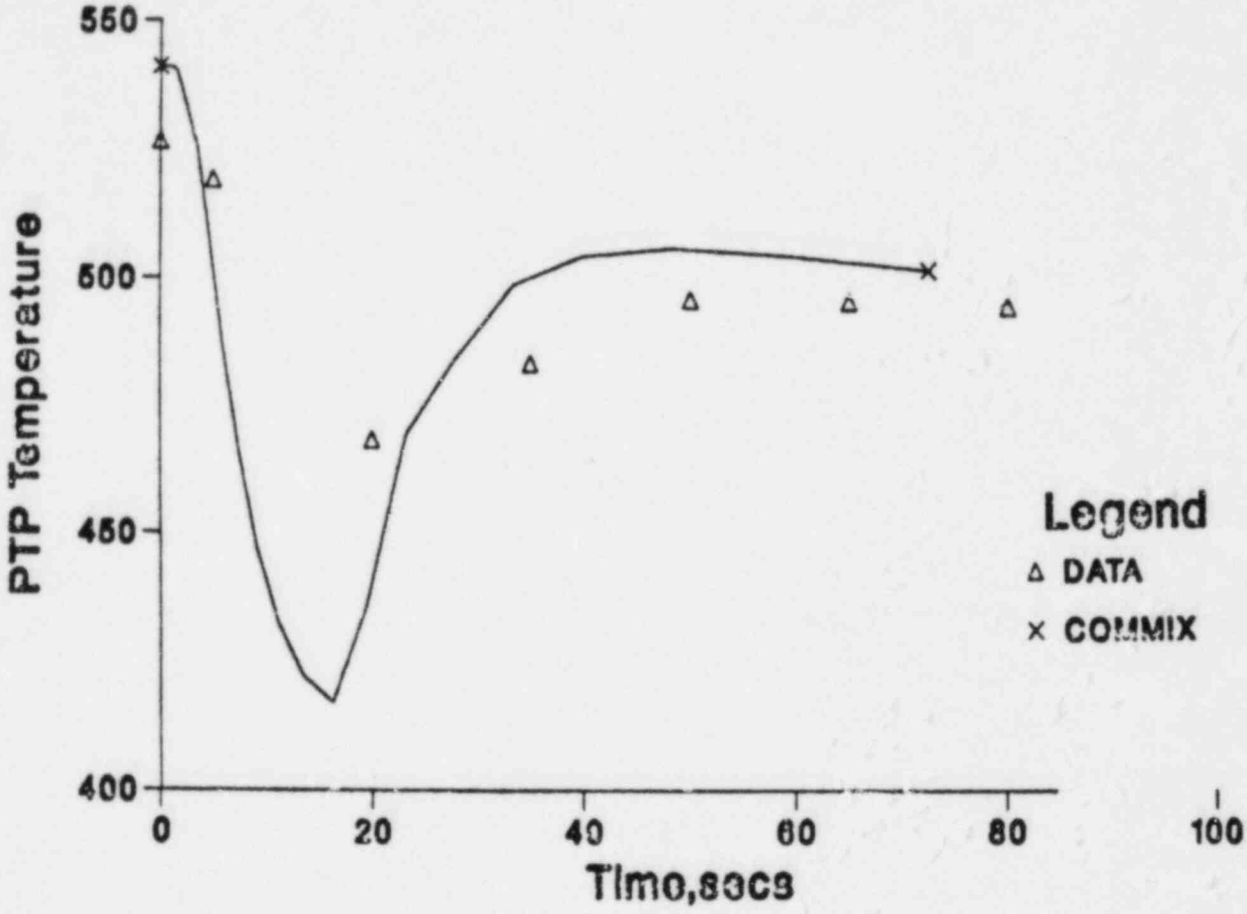

Fig. 20. Comparison of Calculated and Measured PTP Temperatures

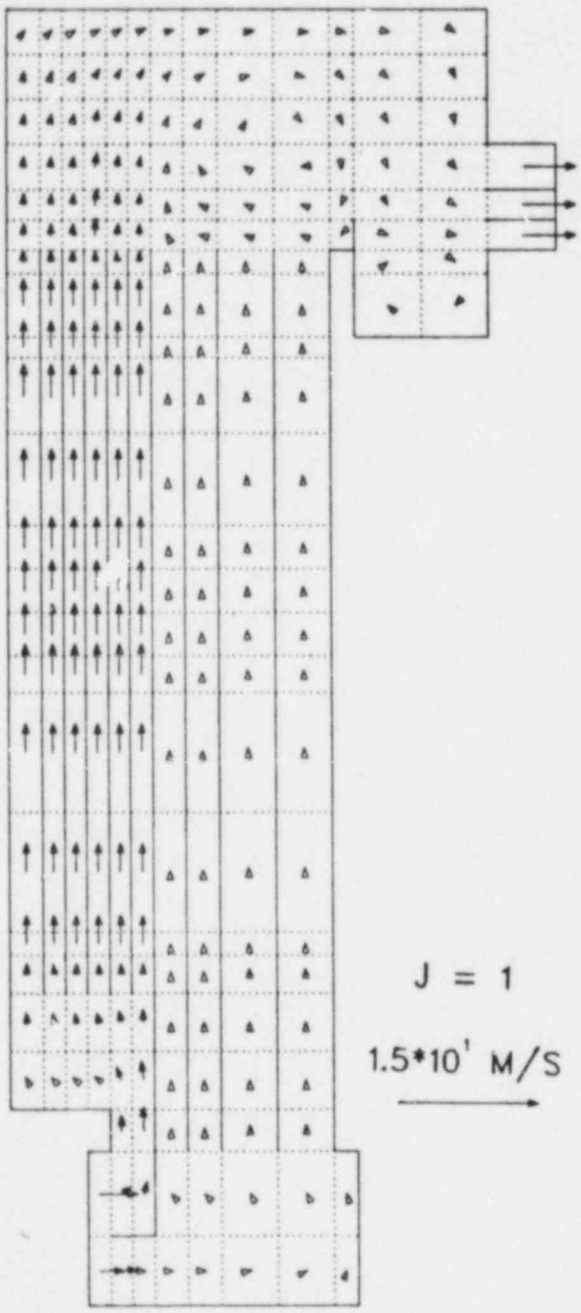

Fig. 21. Steady State Velocity Distribution in the Azimuthal Plane J=1

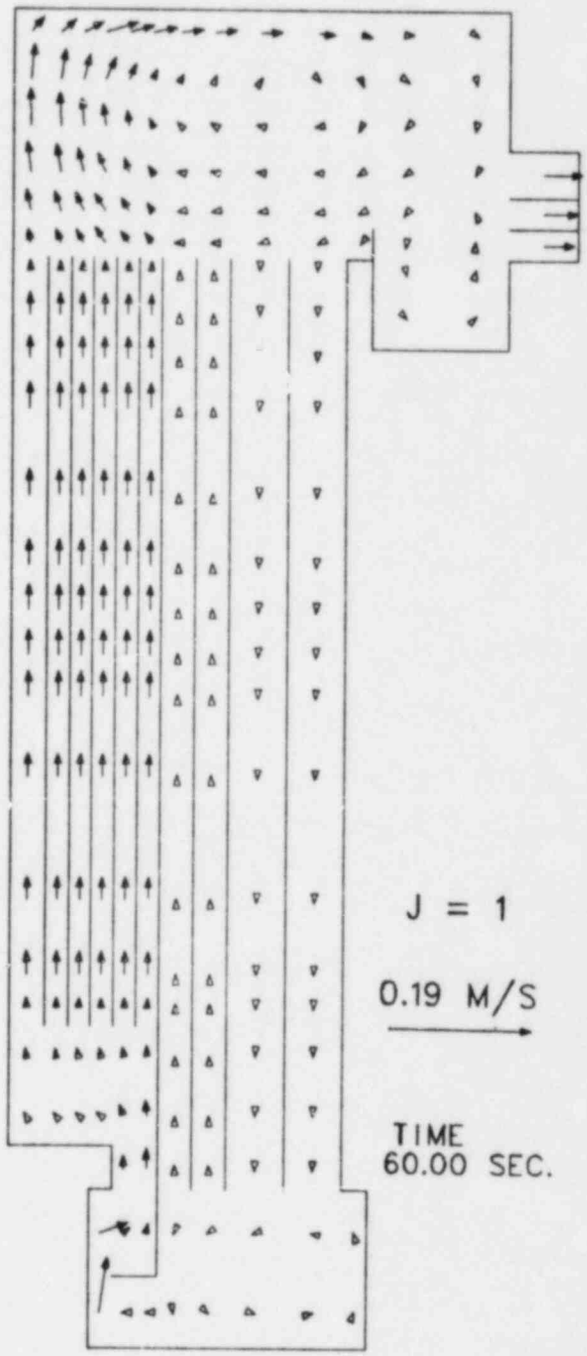

Fig. 22. Velocity Distribution at 60 s of Transient Time

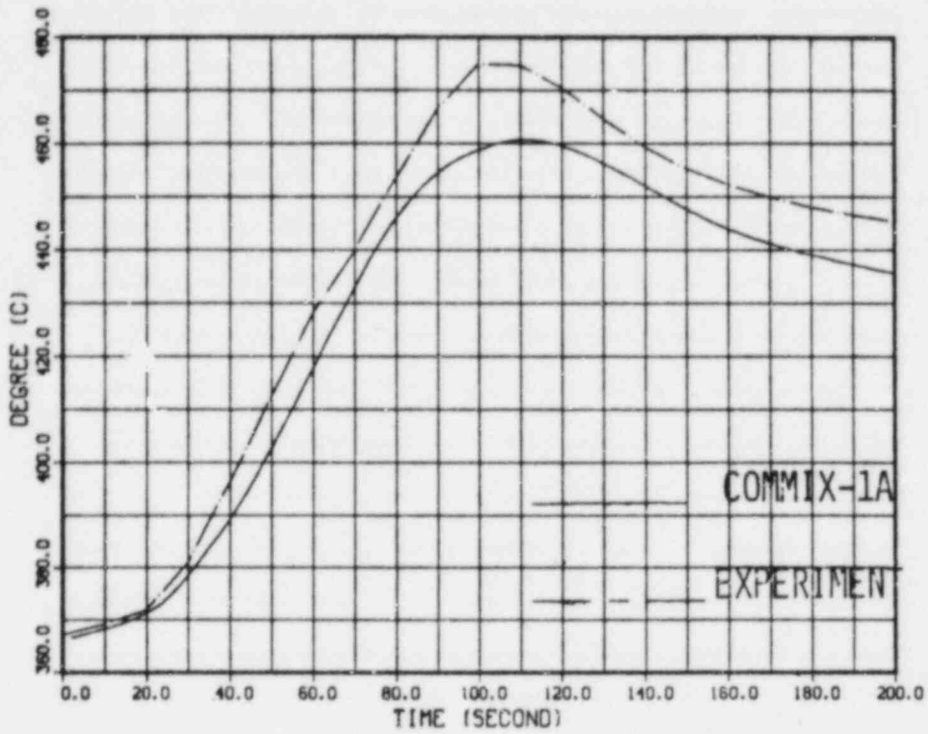

Fig. 23a. Top-of-Core Temperatures for Driver Subassembly XX08

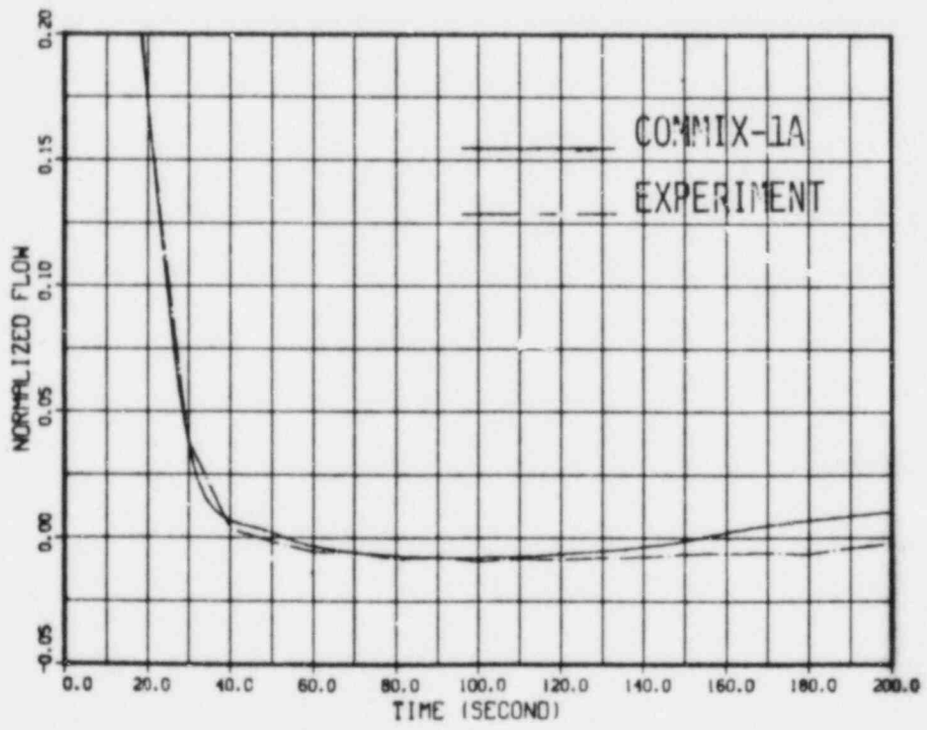

Fig. 23b. Low Pressure Plenum Mass Flow

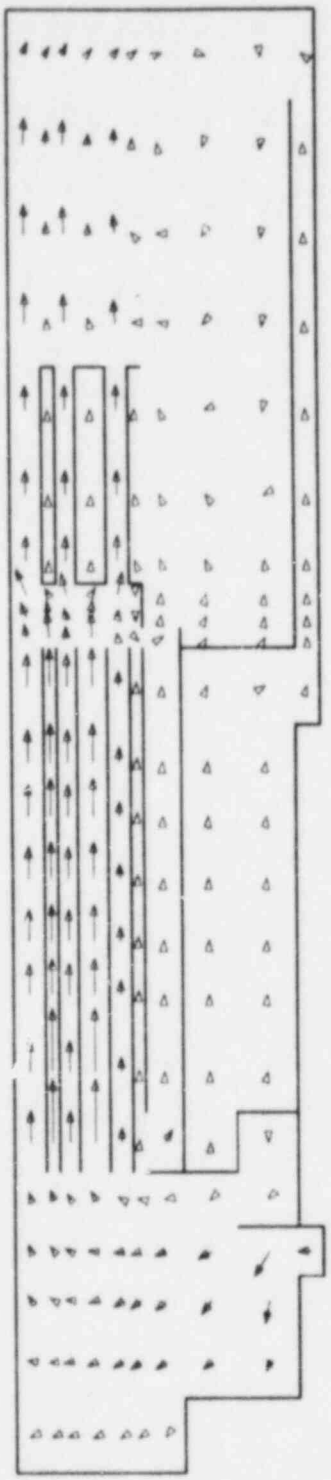

Fig. 24a. Vector Plot Showing Velocity Field in the Plane Normal to Inlet Plane

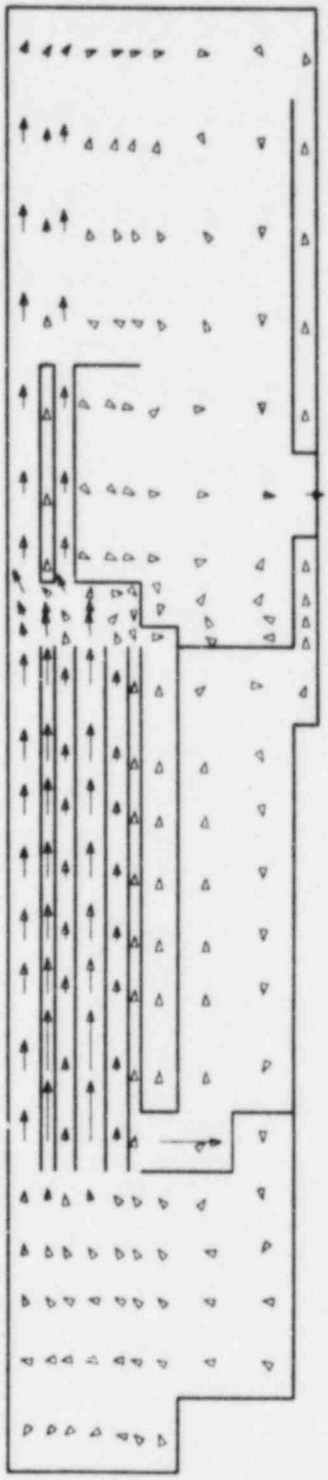

Fig. 24b. Vector Plot Showing Velocity Field in the Plane Normal to Outlet Plane

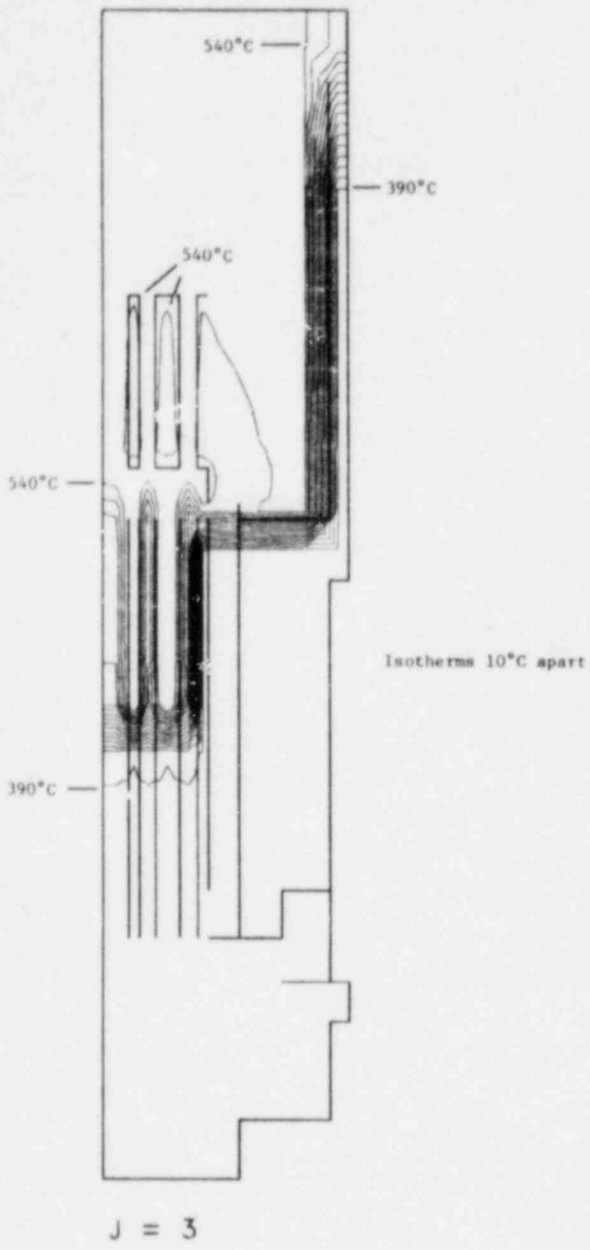

Fig. 25a. Isotherms Showing Temperature Distribution in the Plane Normal to Inlet Plane

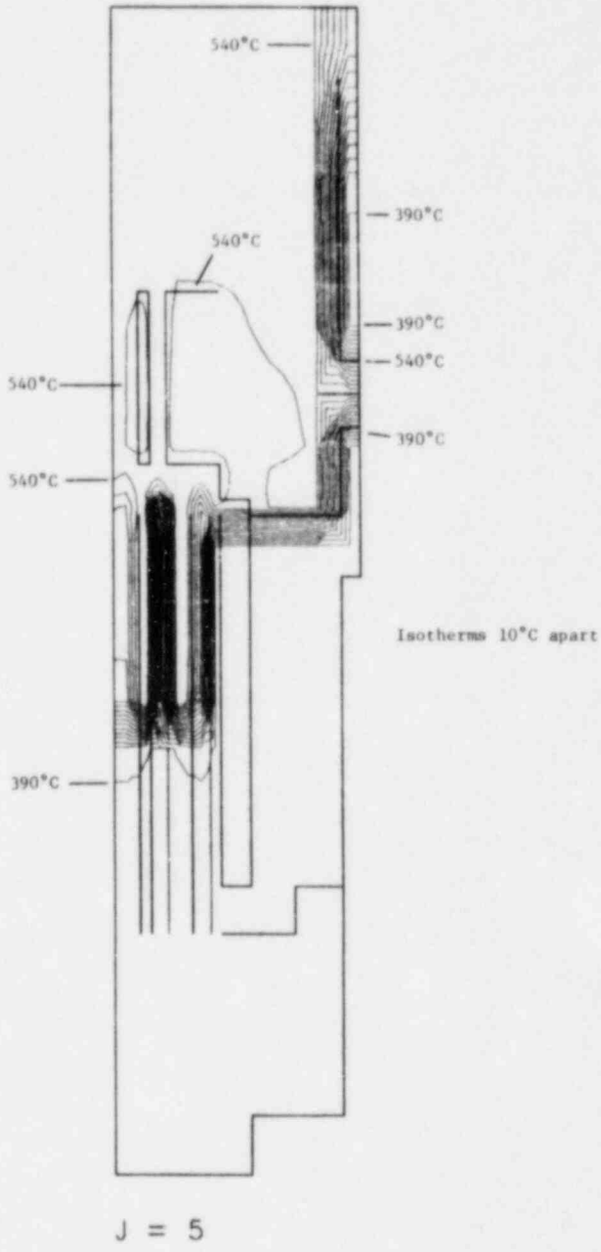

Fig. 25b. Isotherms Showing Temperature Distribution in the Plane Normal to Outlet Plane

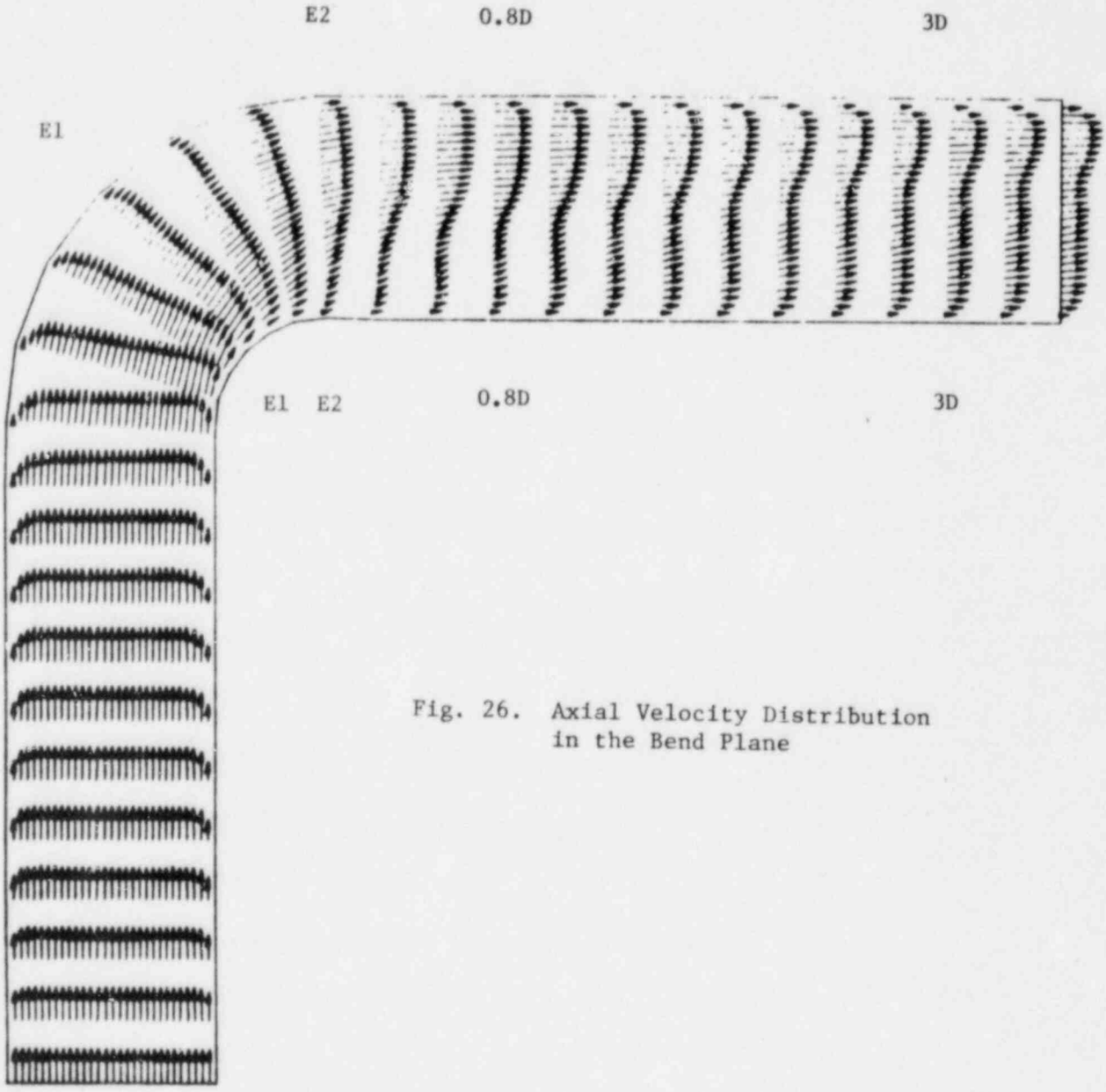

Fig. 26. Axial Velocity Distribution in the Bend Plane

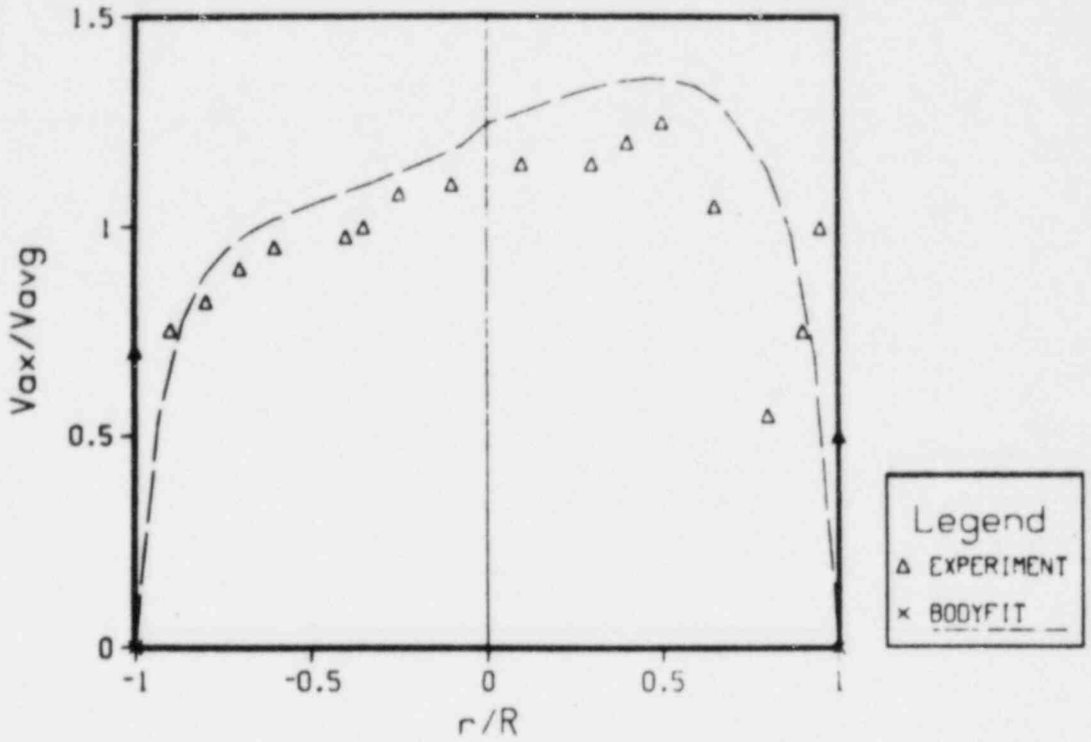

Fig. 27. Axial Velocity in P-Plane at E1-E1

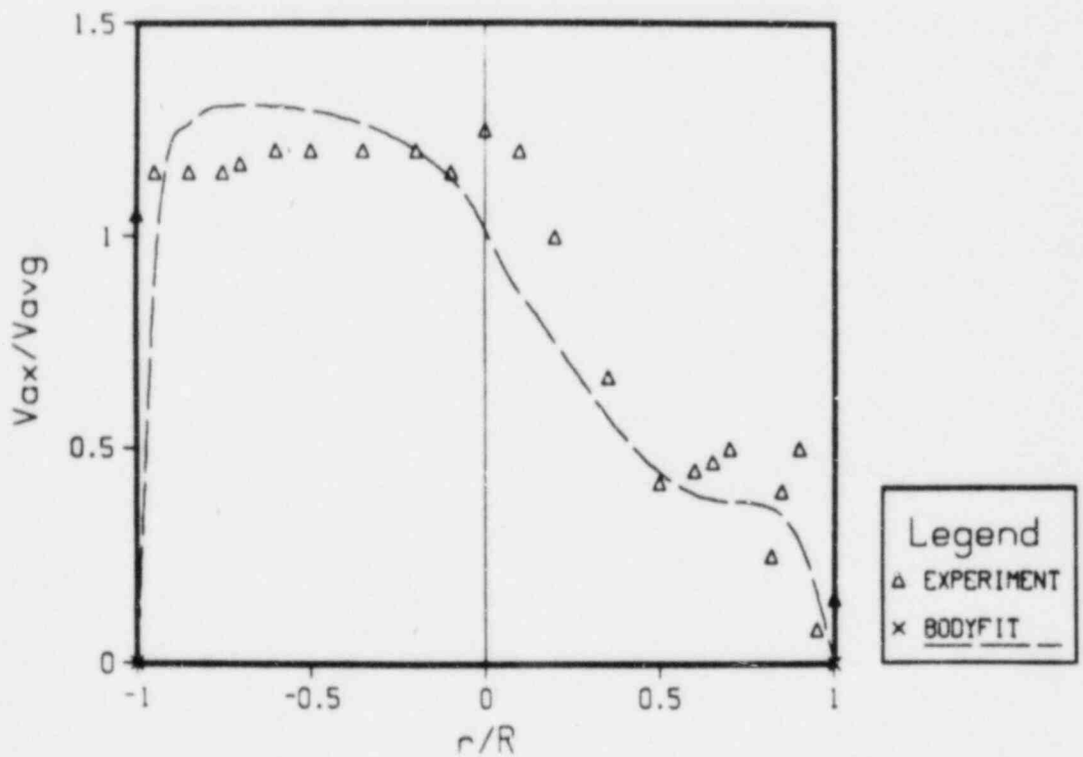

Fig. 28. Axial Velocity in P-Plane at E2-E2

REFERENCES

1. P. A. Pizzica et al., "A User's Guide to EPIC, A Computer Program to Calculate the Motion of Fuel and Coolant Subsequent to Pin Failure in an LMFBR," NUREG/CR-1504, ANL-80-47 (October 1979).

2. H. U. Wider et al., "The PLUTO2 Overpower Excursion Code and a Comparison with EPIC," Proceedings of the ANS/ENS International Meeting of Fast Reactor Safety Technology, Seattle, Washington, August 19-23, 1979, p. 120.

3. Physics of Reactor Safety Quarterly Report, January-March 1982, ANL-82-24 Vol. I, NUREG/CR-2774 Vol. I, p. 6 (1982).

4. S. K. Rhow et al., "An Assessment of HCDA Energetics in the CRBRP Heterogeneous Reactor Cores," CRBRP-GEFR-00523, General Electric Company, Sunnyvale, California, December 1981.

5. R. J. DiMelfi and J. M. Kramer, *Trans. Am. Nucl. Soc.* 39, p. 387 (1981).

6. Op. cit. (Ref. 3), pp. 5-9.

7. Op. cit. (Ref. 3), pp. 2-5.

8. Barbarin and Jones, ASME Vol. 85, J. Basic Eng., 29, 1963.

9. M. C. Chaturvedi, ASCE, J. Hydraulics Division, Vol. 89, 3, 1963, p. 61.

10. Syed and Sturgess, ASME 1980 Meeting, HTD, Vol. 13, p. 71.

11. M. Murakami, Y. Shimizu, and H. Shiragami, "Studies on Fluid Flow in Three-Dimensional Bend Conduits," Bulletin of JSME Vol. 12, No. 54, p. 1369 (1969).

APPENDIX A

IMPORTANT INPUT DATA FOR FFTF SIMULATION

A.1 Dimensions

The dimensions were obtained either from the FSAR or from the design drawings obtained from HEDL. It is not possible and also not relevant to list all design dimensions that were used to simulate the geometry. However, we shall mention below the most important dimensions, which will enable the reader to obtain a picture of the facility.

Vessel Radius	2.911 m
Vessel Height (considered for present calculations)	12.18 m
Inlet-pipe diameter	0.4064 m (16 in.)
Outlet-pipe diameter	0.7112 m (28 in.)
Number of pins per assembly	217
Pin diameter	0.00584 m (0.230 in.)
Number of assemblies (including nonfueled)	91

A.2 Flow Rates and Temperatures

Total inlet flow	2203 kg/s (40,330 gpm)
Inlet temperature	360°C
Outlet temperature	503.3°C

A.3 Boundary Conditions

Inlet	Prescribed velocity and temperature
Outlet	Zero-gradient on outlet velocity and temperature
Walls (outside)	Adiabatic

APPENDIX B

EBR-II Geometric and Operating Characteristics

B.1 Dimensions

Vessel Radius	1.164 m
Vessel Height	3.071 m
Inlet Flow Cross Section	
- HPP	2 x 510 cm^2
- LPP	2 x 82.2 cm^2
Outlet Flow Cross Section	856.3 cm^2
Number of Subassemblies	
- Driver	127
- Reflecor	144
- Blanket	366
Subassembly Details	
- Driver	91 pins, 0.442 cm ϕ
- Reflector	no pins, annular hex geometry
- Blanket	19 pins, 1.252 cm ϕ

B.2 Initial Operating Conditions

Total Power	0.895 MW
Total Inlet Flow	0.507 m^3/s
Inlet Velocity	4.25 m/s
Inlet Temperature	365°C
Average Temperature Increase	~ 1°C
Inlet Pressure	4.265 bars
Outlet Pressure	1.709 bars

Power and Flow Distribution:

	DRIVER	REFLECTOR	BLANKET
Power (%)	76.5	7.8	15.7
Flow (%)	86.5	2	11.5
Power/Flow	0.88	3.9	1.36

B.3 Boundary Conditions

Inlet	Prescribed velocity and temperature
Outlet	Zero gradients on outlet velocity and temperature
Walls	Adiabatic

Distribution for NUREG/CR-2774 Vol. II (ANL-82-24 Vol. II)

Internal:

E. S. Beckjord
C. E. Till
F. S. Onesto
R. Avery
P. B. Abramson
I. Bornstein/
A. B. Klickman
C. E. Dickerman
F. E. Dunn
D. Ferguson/L. Baker
S. H. Fistedis
P. L. Garner
E. Gelbard
H. Henryson
H. H. Hummel (2)
I. T. Hwang
Kalimullah
M. F. Kennedy
D. H. Lennox
L. G. LeSage
D. J. Malloy
A. P. Olson
P. Pizzica
F. G. Prohammer
D. Rose/A. J. Goldman/
J. F. Marchaterre
R. Sevy
J. J. Sienicki
W. J. Sturm
B. J. Toppel
J. B. van Erp
D. Weber
H. Wider
H. M. Domanus
V. L. Shah
B. C-J. Chen
W. T. Sha
P. I. Amundson/
S. G. Carpenter
M. J. Lineberry
D. H. Shaftman
A. Travelli
ANL Contract File
ANL Patent Dept.
ANL Libraries (2)
TIS Files (3)

External:

USNRC, Washington, for distribution per R7 (275)
DOE-TIC, Oak Ridge (2)
Manager, Chicago Operations Office, DOE
President, Argonne Universities Association, Argonne, Ill.
Applied Physics Division Review Committee:
P. W. Dickson, Jr., Clinch River Breeder Reactor Project, Oak Ridge, Tenn. 37830
K. D. Lathrop, Los Alamos National Lab., P. O. Box 1663, Los Alamos, N. M. 87545
D. A. Meneley, Ontario Hydro, 700 University Ave., Toronto, Canada M5G 1X6
J. E. Meyer, Massachusetts Inst. Technology, Cambridge, Mass. 02139.
R. Sher, Stanford U., Stanford, Calif. 94305
C. Spight, AMAF Industries, Inc., P. O. Box 1100, Columbia, Md. 21044
D. B. Wehmeyer, The Detroit Edison Co., 2000 Second Ave., Detroit, Mich. 48226
Components Technology Division Review Committee:
A. A. Bishop, U. Pittsburgh, Pittsburgh, Pa. 15261
F. W. Buckman, Consumers Power Co., 1945 Parnall Rd., Jackson, Mich. 49201
R. Cohen, Purdue U., West Lafayette, Ind. 47907
R. A. Greenkorn, Purdue U., West Lafayette, Ind. 47907
W. M. Jacobi, Westinghouse Electric Corp., Nuclear Fuel Div., Pittsburgh, Pa. 15230
E. E. Ungar, Bolt, Beranek and Newman Inc., 50 Moulton St., Cambridge, Mass. 02138
J. Weisman, U. Cincinnati, Cincinnati, O. 45221
C. Erdman, Texas A&M U., College Station, Tex. 77843
K. O. Ott, Purdue U., West Lafayette, Ind. 47907
R. Lancet, Atomics International, P. O. Box 309, Canoga Park, Calif. 91304